q_T subtraction for jets: a study of Higgs plus jet at NLO

Master thesis

Author
Mark N. Costantini

Supervisors
Prof. Dr. Massimiliano Grazzini
Dr. Luca Buonocore, Dr. Luca Rottoli

Universität Zürich[UZH]

Department of Theoretical Physics
University of Zürich

August 2021

Abstract

In this thesis we present a new NLO QCD calculation of Higgs plus jet production at the LHC. We use the recently developed extension of the q_T subtraction formalism to cancel the IR divergences for each sub-processes [1]. This method exploits the observation that the transverse momentum of the Higgs boson plus jet system completely describes the singularity structure of QCD when final-state coloured particles are present. In particular we stress that the subtraction works at arbitrary values of the jet radius while the jet-function, i.e. the clustered final state radiation contributions, is currently known in the small R limit only. Our NLO results, for small jet radius values ($R \leq 0.1$), nicely agree with those obtained by an independent computation performed with local subtraction, both for the inclusive cross section and several differential distributions.

·_ _·· ·_ ·· _·· ·_

Contents

1 Introduction

Particle colliders are one of the main tools used to understand the structure of fundamental physics. In particular, they are the best known strategy to date for studying heavy objects that are short-lived and rarely produced. The Large Hadron Collider (LHC), at Cern, is the largest and most powerful particle accelerator in the world. Inside the accelerator, two beams of high-energy hadrons (protons or heavy ions) travel almost at the speed of light before being collided. The high energy and high luminosity (a measure of the number of potential collisions per unit area in a given period of time) of the LHC allows the study of very rare and short-lived massive particles and, in particular, allowed in July 2012 the discovery of a new boson with a mass close to 125 GeV. This particle is consistent with the Higgs boson predicted by the Brout-Higgs-Englert mechanism [2–4] and its discovery was therefore an extraordinary achievement for the high-energy physics community.

Nowadays, the Higgs boson still plays a leading role in the searches for new physics at the LHC. In particular, altough the run I and II measurements at LHC showed that the new resonance is compatible with the Standard Model (SM) Higgs boson, there still is the possibility that more precise measurements will uncover small deviations from the SM predictions.

During run I and II differential Higgs observables were measured, altough still with relatively large uncertainties. Among these observables, a prominent role is played by the transverse momentum spectrum (p_T) of the Higgs boson, whose study could shed light on the structure of the Higgs sector. For instance, evidence of new physics could emerge either as distortions of its shape due to modified light Yukawa couplings [5, 6] or as deviations in the tail of the differential distributions [7].

At the LHC, Higgs with high transverse momentum are typically accompained by high transverse momentum jets. The precise calculation, i.e. the computation of higher order corrections to the production cross section of the Higgs plus jet process within perturbative Quantum Field Theory (QFT), is therefore of crucial importance for the high-precision program. At present, many different techniques allowing for the computation of higher order corrections to LHC observables have been developed and succesfully applied to different kind of processes. The current state of the art for the Higgs plus jet observable is next-to-next-to-leading order (NNLO) in Quantum-Chromo-Dynamics (QCD). This computation has been performed in Ref. [8] using the N-jettiness event-shape variable, in Ref. [9] using sector-improved residue subtraction and in Ref. [10] with the antenna subtraction method.

Another method that is well suited for higher order corrections to LHC observables is q_T-subtraction (see Ref. [11]) that was originally formulated for colour singlet production (see Ref. [12] for the actual implementation of many on- and off-shell colour singlet processes). In the last few years q_T-subtraction has been extended for coloured massive final states and applied to top-quark and bottom-quark pair production at NNLO in the works [13] and [14]. The NNLO production of $t\bar{t}H$ for the flavour off-diagonal channels has also been computed in Ref. [15]. Very recently, q_T-subtraction has been applied to next-to-leading order (NLO) Electroweak (EW) and mixed QCD-EW corrections for Drell-Yan processes in the works [16] and [17].

Until now, however, q_T-subtraction has never been applied to processes with jets in

the final state. The main goal of this thesis is to compute the NLO corrections to the Higgs plus jet process by extending the q_T-subtraction formalism to deal with these processes.
The thesis is organized as follows. In chapter (2) we will briefly discuss the appearance and the main properties of infrared (IR) divergences in Quantum Chromo Dynamics (QCD), relevant for the computation of IR safe observables. In chapter (3) we will introduce the q_T-subtraction method and illustrate its main keypoints trough the explicit example of Higgs production in gluon-gluon fusion at NLO. Chapter (4) and (5) are devoted to the presentation of the Higgs plus jet computation at NLO. Finally, in chapter (6) we present our conclusions.

2 Infrared singularities in Quantum Chromo Dynamics

The infrared divergences are a general property of gauge theories with massless particles. In QCD, these divergences are associated with regions of phase space where a real or a virtual gluon has vanishing four-momentum (**soft**) or becomes **collinear** to another massless parton.
To better illustrate the appearance of these divergences in QCD we consider the order $\alpha_s = \frac{g_s^2}{4\pi}$ (g_s is the strong coupling) corrections to the production of hadrons in electron-positron collisions, namely $e^+e^- \to$ hadrons. This reaction proceeds via e^+e^- annihilation into a quark-anti-quark pair at lowest order. The Born process, shown in figure (1), is a purely Quantum Electrodynamics (QED) process whose cross section is given by

$$\sigma_{q\bar{q}}^{\text{Born}} = \frac{4\pi\alpha^2}{Q^2} N_c \sum_q e_q^2 \,, \tag{1}$$

where the sum runs over the different flavours of the quarks, α is the QED coupling, N_c ($= 3$) accounts for all possible colour states, $Q^2 = 2p_1 \cdot p_2$ is the centre of mass energy of the e^+e^- pair and e_q are the electrical charges of the quarks in unit of electron charge. The order α_s corrections to the cross section are given by diagrams in which a real gluon is emitted in the final state, and diagrams in which a virtual gluon is exchanged (interfered with a Born graph) as depicted in figure (2). The real and virtual contributions are both separately divergent in the unresolved limits and give a finite, and thus physical, result only after being combined together. Unresolved means that the energy of the gluon is much smaller than the energy (Q) involved in the process or that the gluon is emitted almost parallel to one of the two fermions and cannot therefore be distinguished from it. For the sake of clarity, we will now consider the case where the emitted real gluon has vanishing energy (note that since the gluon is massless, this is equvalent to $k^\mu \to 0$). The sum of the amplitudes for the emission of a gluon from the quark and antiquark respectively in the $k^\mu \to 0$ limit is given by

$$i\mathcal{M}_{\text{soft}}(e^+e^- \to q\bar{q} + g) = (i\mathcal{M}_{\text{B}}) \times (-g_s t^a) \left\{ \frac{q_1 \cdot \epsilon(k)}{q_1 \cdot k} - \frac{q_2 \cdot \epsilon(k)}{q_2 \cdot k} \right\}. \tag{2}$$

Where $\mathcal{M}_{\text{B}}$ represents the amplitude for the Born process and t^a is the generator of the fundamental $SU(3)_c$ representation. Taking the square and averaging (summing)

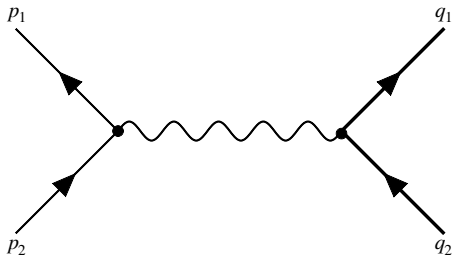

Figure 1: Leading order Feynman diagram for e^+e^- to hadrons

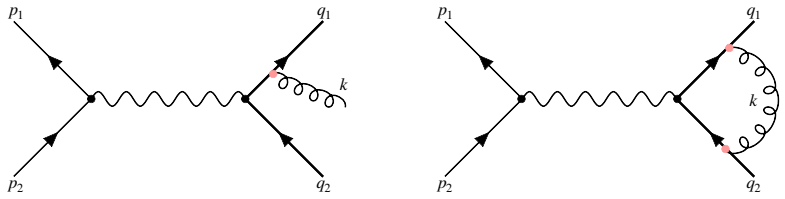

Figure 2: Real gluon emission (left graph) and virtual gluon exchange in e^+e^- annihilation

over the initial (final) state quantum numbers we get

$$|\mathcal{M}_{\text{soft}}|^2 = |\mathcal{M}_{\text{B}}|^2 C_F g_s^2 \frac{2q_1 \cdot q_2}{(q_1 \cdot k)(q_2 \cdot k)}, \tag{3}$$

where C_F ($= \frac{N_c^2-1}{2N_c} = \frac{4}{3}$) is the Casimir of the fundamental $SU(3)_c$ representation. In particular, it is important to note the factorised form of the squared amplitude. This, as we are going to show in more detail in section (2.2), is a general feature of the soft emissions[1]. From the squared amplitude we turn to the cross section by supplying the phase space factor for the gluon

$$\sigma_{q\bar{q}g} = C_F g_s^2 \sigma_{q\bar{q}}^{\text{Born}} \int \frac{d^3\vec{k}}{2k^0(2\pi)^3} \frac{2q_1 \cdot q_2}{(q_1 \cdot k)(q_2 \cdot k)}. \tag{4}$$

Let us now consider the process in the rest frame of the virtual photon and let us call θ the angle between the gluon and the quark 3-momenta. We have then

$$\sigma_{q\bar{q}g} = C_F \frac{\alpha_s}{2\pi} \sigma_{q\bar{q}}^{\text{Born}} \int d\cos\theta \frac{dk^0}{k^0} \frac{4}{(1-\cos\theta)(1+\cos\theta)}\ . \tag{5}$$

The cross section for producing an extra gluon is therefore divergent in three regions

- when the emitted gluon has vanishing energy ($k^0 \to 0$),
- when the emitted gluon is parallel to the direction of the quark ($\cos\theta = 1, \theta = 0$),
- when the emitted gluon is parallel to the direction of the antiquark ($\cos\theta = -1, \theta = \pi$).

The first divergence is called **soft** while the last two are called **collinear**. Both divergences are of infrared type. As already stated above, the sum of the real and virtual corrections of order α_s to the production of hadrons in e^+e^- annihilation is finite. It follows that the virtual corrections must have the same kind of singularities, with opposite sign. This cancellation is a consequence of a general theorem in quantum mechanics, the Kinoshita-Lee-Nauenberg (KLN) theorem [18] [19]. Roughly speaking, the theorem

[1] Note that in presence of more than three coloured particles at Born level, strict factorisation does not hold because of non trivial soft colour-correlations.

deals with divergences that arise because of degeneracy in the final state. For example, the final state with an extra soft gluon is nearly degenerate with the state with no gluons at all, and the state with a quark split up into a quark plus a gluon, with parallel momenta, is degenerate with the state with no radiation at all. The theorem states that the cross section obtained by summing up over degenerate states are not divergent.

2.1 Jet cross sections

At the beginning of this chapter, we briefly discussed the production of a quark-antiquark pair in e^+e^- annihilation. As already argued, its cross section is not physically meaningful, since coloured partons are never observed in the final state. A physically more meaningful quantity is the cross section for e^+e^- to hadrons. One must therefore define a cross-section that is calculable and finite in perturbation theory and that in some way characterises the hadronic final state. A possible observation is that the distribution of the final state hadrons should be reminiscent of that of the "hard" partons described by perturbation theory. Soft and collinear partons are copiously produced in all-order QCD, leading to configurations characterised by sprays or clusters of hadrons, called jets, along the direction of the hard partons. Many different definitions of jets exist in the literature and all of them are based on a so-called jet-algorithm. Jet algorithms provide a set of rules for grouping particles into jets. They usually involve one or more parameters that indicate how close two particles need to be in order to belong to the same jet. The first definition of jets, designed for e^+e^- collision processes, goes back to Sterman and Weinberg [20] and reads as follows. A hadronic event in e^+e^- collisions, with centre-of-mass energy Q, contributes to the Sterman-Weinberg 2-jet cross section if we can find two cones with opening angle δ containing all the energy of the event except at most a fraction $\epsilon \ll 1$ of the total energy. We distinguish three contributions

(a) the virtual cross section contributes to the 2-jet cross section, irrespective of the value of ϵ and δ .

(b) The real cross section, with one gluon emission, when the energy of the emitted gluon k^0 is limited by $k^0 < \epsilon Q$, contributes to the 2-jet cross section.

(c) The real cross section, when $k^0 > \epsilon Q$, when the emission angle with respect to the quark (or antiquark) is less than δ, contributes to the 2-jet cross section.

The contributions are

$$\sigma_a = -\sigma_{\text{Born}} \frac{2\alpha_s}{\pi} C_F \int_0^Q \frac{dk^0}{k^0} \int_{-1}^{1} \frac{d\cos\theta}{1-\cos^2\theta}, \tag{6}$$

$$\sigma_b = \sigma_{\text{Born}} \frac{2\alpha_s}{\pi} C_F \int_0^{\epsilon Q} \frac{dk^0}{k^0} \int_{-1}^{1} \frac{d\cos\theta}{1-\cos^2\theta}, \tag{7}$$

$$\sigma_c = \sigma_{\text{Born}} \frac{2\alpha_s}{\pi} C_F \int_{\epsilon Q}^{Q} \frac{dk^0}{k^0} \left[\int_{\cos\delta}^{1} \frac{d\cos\theta}{1-\cos^2\theta} + \int_{-1}^{\cos(\pi-\delta)} \frac{d\cos\theta}{1-\cos^2\theta} \right]. \tag{8}$$

Summing the three contributions plus the Born cross section together we get a 2-jet cross section that depends on the two parameters ϵ and δ

$$\sigma_{2\text{-jet}}(\epsilon, \delta) = \sigma_{\text{Born}} \left(1 - \frac{4\alpha_s}{\pi} C_F \log(\epsilon) \log(\frac{\delta}{2}) + \mathcal{O}(\alpha_s^2) \right). \tag{9}$$

In particular the result is finite meaning that all the divergent pieces canceled out. This follows from the fact that the Sterman-Weinberg jet algorithm, at order α_s, allows one to sum up over all degenerate states leading thus to an IR safe observable. The Sterman-Weinberg algorithm, while giving a physically clean picture, is however no longer used since not well suited for analysing multi-jet final states. Reconnecting to the actual process under consideration in this thesis, we will now introduce a set of jet-algorithms that is widely used in hadron-hadron collisions and that is part of a larger class of algorithms called sequential recombination jet algorithms (see ref [21] for more details).

2.1.1 k_T type algorithms with incoming hadrons

The main idea in sequential recombination algorithms is to introduce a measure of distance d_{ij} between two particles i and j and a jet resolution threshold d_{cut}. The algorithm then works as follows

1. compute the distances d_{ij} between all the pairs of particles i, j,
2. find the minimal d_{ij},
3. if $d_{ij} < d_{\text{cut}}$ recombine the two particles into a single particle and go back to step 1,
4. if $d_{ij} > d_{\text{cut}}$ stop the algorithm and classify all particles as jets.

Additionally one has to define a recombination scheme, which indicates what momentum to assign to the combination of two particles, the simplest is the 4-vector sum.
In hadron-hadron collisions an additional precaution needs to be taken due to the fact that divergences in the QCD branching probabilities are not just between pairs of outgoing particles, but also between an outgoing particle and the incoming beam direction (see section (2.3) for more details). This can be taken into account by introducing the idea of an additional particle-beam distance d_{iB}. Moreover, in hadronic collisions, it is standard to use variables that are invariant under longitudinal boosts (such as the transverse momentum and the rapidity).
To cluster the particles in k_T-algorithms, one can introduce a general class of distance measures in momentum space, each classified by an integer p, namely

$$\begin{aligned} d_{iB} &= (p_{\perp,i})^{2p} \quad \text{for each parton i,} \\ d_{ij} &= \min(p_{\perp,i}^{2p}, p_{\perp,j}^{2p}) \frac{\Delta R_{ij}^2}{R_0^2} \quad \text{for each parton pair } i, j. \end{aligned} \tag{10}$$

Where

$$\Delta R_{ij} = (y_i - y_j)^2 + (\phi_i - \phi_j)^2, \tag{11}$$

denotes the distance between the two particles i and j in the rapidity-azimuth space and R_0 plays the role of a jet resolution threshold in the sense that two particles are not recombined togheter if their distance is greater then R_0.
By now we have motivated the appearance of IR divergences in perturbative QCD calculations. Moreover we have explicitly shown, by means of the $e^+e^- \to$ jets example, how one needs to define physical observables in order for this divergences to cancel. In the following section we will describe the behaviour of QCD matrix elements at order α_s in the soft and collinear limits, i.e. we will present the well-known factorisation formulae (see Ref. [22]). The knowledge of these limits is fundamental for the computation of higher order cross-section corrections because it allows one to isolate the singularities of the cross-sections in the intermediate steps of the computation, i.e. in the separate computation of real and virtual contributions.

2.2 Infrared factorisation of QCD amplitudes

We consider a process characterised by m partons, with momenta $p_1, \ldots, p_m$, in the final state at lowest order. We denote the corresponding tree level matrix element as $\mathcal{M}_m$. The matrix element has the following structure

$$\mathcal{M}^{c_1,\ldots,c_m;s_1,\ldots,s_m}_{a_1,\ldots,a_m} \tag{12}$$

where $\{c_1, \ldots c_m\}$, $\{s_1, \ldots s_m\}$ and $\{a_1, \ldots a_m\}$ respectively denote the colour, spin and flavour of the m final state QCD partons.
In the following we use the conventional dimensional regularisation (CDR) with $d = 4 - 2\epsilon$ space-time dimensions and consider two helicity states for the fermions and $d - 2$ helicity states for the gluons.
We also define the spin-polarisation tensor

$$\mathcal{T}^{s_1,s_1'}_{a_1,\ldots,a_m} = \sum_{\text{spins}\neq s_1,s_1'} \sum_{\text{colours}} \mathcal{M}^{c_1,\ldots,c_m;s_1,\ldots,s_m}_{a_1,\ldots,a_m} \left[\mathcal{M}^{c_1,\ldots,c_m;s_1',\ldots,s_m}_{a_1,\ldots,a_m}\right]^\dagger \tag{13}$$

which is the square of the matrix element (12) summed over all spin and colours apart from s_1.

2.2.1 Factorisation in the collinear limit

We consider now the limit in which two of the final state QCD partons, say p_1 and p_2, become collinear to each other. This limit can be precisely defined as follows

$$\begin{aligned} p_1^\mu &= z p^\mu + k_\perp^\mu - \frac{k_\perp^2}{z}\frac{n^\mu}{2p\cdot n} \quad , \quad p_2^\mu = (1-z)p^\mu - k_\perp^\mu - \frac{k_\perp^2}{1-z}\frac{n^\mu}{2p\cdot n} \quad , \\ s_{12} &\equiv 2p_1\cdot p_2 = -\frac{k_\perp^2}{z(1-z)} \quad , \qquad k_\perp \to 0 \quad . \end{aligned} \tag{14}$$

In equation (14) we introduce the Sudakov decomposition: the lightlike ($p^2 = 0$) vector p^μ denotes the collinear direction while n^μ is an auxiliary light-like vector needed to fix one of the four degrees of freedom of the p_1, p_2 four-vectors.
In the small $k_\perp$ limit (i.e. neglecting terms that are less singular then $1/k_\perp^2$), the square of the matrix element (12) fulfils the factorisation formula

$$|\mathcal{M}_{a_1,a_2,\dots}(p_1,p_2,\dots)|^2 \simeq \frac{2}{s_{12}}\, 8\pi\mu^{2\epsilon}\alpha_s\, \mathcal{T}^{ss'}_{a,\dots}(p,\dots)\, \hat{P}^{ss'}_{a_1a_2}(z,k_\perp;\epsilon) \quad , \tag{15}$$

where μ is the dimensional regularisation scale. The spin polarisation tensor is obtained by replacing the partons a_1 and a_2 with a single parton denoted by a.
The parton a carries the quantum numbers of $a_1 + a_2$ in the collinear limit. Thus, its momentum is p^μ and its other quantum numbers are obtained according to the following rule: gluon + anything gives anything and quark + antiquark gives gluon.
The kernel $\hat{P}^{ss'}_{a_1a_2}(z,k_\perp;\epsilon)$ is the d-dimensional Altarelli-Parisi (AP) splitting function. The explicit expression for the splitting functions is (at 1 loop)

$$\hat{P}^{ss'}_{qq}(z;\epsilon) = \hat{P}^{ss'}_{\bar{q}\bar{q}}(z,k_\perp;\epsilon) = \delta_{ss'}\,\frac{C_F}{2}\left[\frac{1+z^2}{1-z} - \epsilon(1-z)\right] \quad , \tag{16}$$

$$\hat{P}^{ss'}_{gq}(z;\epsilon) = \hat{P}^{ss'}_{g\bar{q}}(z,k_\perp;\epsilon) = \delta_{ss'}\,\frac{C_F}{2}\left[\frac{1+(1-z)^2}{z} - \epsilon z\right] \quad , \tag{17}$$

$$\hat{P}^{\mu\nu}_{qg}(z,k_\perp;\epsilon) = \hat{P}^{\mu\nu}_{\bar{q}g}(z,k_\perp;\epsilon) = \frac{T_R}{2}\left[-g^{\mu\nu} + 4z(1-z)\frac{k_\perp^\mu k_\perp^\nu}{k_\perp^2}\right] \quad , \tag{18}$$

$$\hat{P}^{\mu\nu}_{gg}(z,k_\perp;\epsilon) = \frac{1}{2}2C_A\left[-g^{\mu\nu}\left(\frac{z}{1-z} + \frac{1-z}{z}\right) - 2(1-\epsilon)z(1-z)\frac{k_\perp^\mu k_\perp^\nu}{k_\perp^2}\right] \quad . \tag{19}$$

The AP kernels can be considered as matrices acting on the spin indices s, s' of the spin polarisation tensor. In particular note that the splitting functions (16) and (17) originating from the splitting of a fermion are proportional to the unity matrix in the spin indices. The splitting functions (18) and (19) instead, originating from the splitting of a gluon have an explicit $k_\perp-$ dependence producing non-trivial azimuthal dependence with respect to the directions of the other momenta in the factorised matrix element.
Equations (16)–(19) lead to the more familiar form of the d-dimensional splitting functions only after average over the polarisations of the parton a. This is obtained by means of the factors

$$\frac{1}{2}\delta_{ss'} \tag{20}$$

for a fermion, and (the gauge terms are proportional either to p^μ or to p^ν)

$$\frac{1}{d-2}d_{\mu\nu}(p) = \frac{1}{2(1-\epsilon)}(-g_{\mu\nu} + \text{gauge terms}) \tag{21}$$

with

$$-g^{\mu\nu}d_{\mu\nu}(p) = d-2\,, \qquad p^\mu\, d_{\mu\nu}(p) = d_{\mu\nu}(p)\, p^\nu = 0\,, \tag{22}$$

for a gluon with on-shell momentum p.
Denoting by $\langle \hat{P}_{a_1 a_2} \rangle$ the average of $\hat{P}_{a_1 a_2}$ over the polarisations of the parent parton a, we have:

$$\langle \hat{P}_{qq}(z;\epsilon) \rangle = \langle \hat{P}_{\bar{q}\bar{q}}(z;\epsilon) \rangle = \frac{C_F}{2} \left[\frac{1+z^2}{1-z} - \epsilon(1-z) \right] , \tag{23}$$

$$\langle \hat{P}_{gq}(z;\epsilon) \rangle = \langle \hat{P}_{g\bar{q}}(z;\epsilon) \rangle = \frac{C_F}{2} \left[\frac{1+(1-z)^2}{z} - \epsilon z \right] , \tag{24}$$

$$\langle \hat{P}_{qg}(z;\epsilon) \rangle = \langle \hat{P}_{\bar{q}g}(z;\epsilon) \rangle = \frac{T_R}{2} \left[1 - \frac{2z(1-z)}{1-\epsilon} \right] , \tag{25}$$

$$\langle \hat{P}_{gg}(z;\epsilon) \rangle = \frac{1}{2} 2C_A \left[\frac{z}{1-z} + \frac{1-z}{z} + z(1-z) \right] . \tag{26}$$

2.2.2 Factorisation in the soft limit

In the following we consider the emission of a soft, i.e. with vanishing four-momentum, gluon off a hard parton.
Unlike for the collinear radiation, the soft gluon emission does not change the momentum of the radiating parton. However, since the gluon carries a colour, it will change the colour of the emitter. This leads to non-trivial colour correlations between the matrix elements.
To discuss the soft factorisation formulas we consider the same general QCD process as in Eq. (12) assuming that one of the partons, say p_1, is a gluon. In particular we consider the case in which the gluon becomes soft and is emitted by an external leg. Internal lines that go on-shell do not lead to a soft singularity and therefore will not be considered.
The general factorisation formula of the matrix element (12) in the $p_1^\mu \to 0$ limit can be written as

$$\mathcal{M}^a(p_1; p_2, \ldots, p_m) \simeq i g_s \mu^\epsilon \epsilon_\mu(q) J^{\mu,a} \mathcal{M}(\{p_i\}), \tag{27}$$

where $J^{\mu,a}$ is called Eikonal current and is defined as

$$J^{\mu,a} = \sum_{i=1}^{m} T_i^a \frac{p_i^\mu}{p_i \cdot p_1} . \tag{28}$$

The factor T_i^a is a general "colour operator" and depends on whether the emitter is a gluon or a fermion. In particular we have

$$T^a_{cc'} = \begin{cases} t^a_{cc'} & \text{outgoing } q \text{ or incoming } \overline{q}, \\ -t^{\dagger a}_{cc'} & \text{outgoing } \overline{q} \text{ or incoming } q, \\ i f_{cac'} & \text{gluon.} \end{cases} \tag{29}$$

Moreover colour conservation is expressed as

$$\sum_i T_i^a = 0 . \tag{30}$$

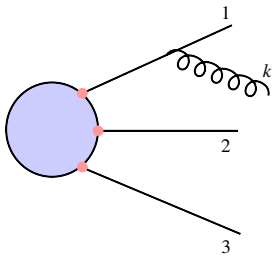

Figure 3: Process with 3 hard coloured partons and one soft gluon

By squaring Eq. (27) and summing over the gluon polarisations we arrive at the well-known soft-gluon factorisation formula for the squared tree-level amplitude:

$$|\mathcal{M}(p_1; p_2, \ldots, p_m)|^2 \simeq g_s^2 \mu^{2\epsilon} 2 \sum_{i,j} T_i^a T_j^a \mathcal{S}_{ij}(p_1) |\mathcal{M}(p_2, \ldots, p_m)|^2, \tag{31}$$

where $\mathcal{S}_{ij}(p_1)$ is the eikonal function and is given by

$$\mathcal{S}_{ij}(p_1) = \frac{p_i \cdot p_j}{2(p_i \cdot p_1)(p_j \cdot p_1)}. \tag{32}$$

The product of the colour operators on the right-hand side of Eq. (31) can in some special cases be expressed as a linear combination of Casimir invariants of the colour group. In these cases we say that the algebra "closes". In particular, the algebra "closes" when there are three or fewer coloured hard partons.
To illustrate this we consider a general process with three emitting partons (gluons or quarks) p_1, p_2, p_3 and additional soft radiation k as shown in Figure (3). Using the colour conservation formula in Eq. (30) we can write

$$2T_i T_j = T_k^2 - T_i^2 - T_j^2 \text{ , with } (i, j, k) \in \{1, 2, 3\} \tag{33}$$

$$T_i^2 = \begin{cases} C_F & \text{if parton } i \text{ is a quark or antiquark,} \\ C_A & \text{if parton } i \text{ is a gluon.} \end{cases} \tag{34}$$

Equation (31) then becomes

$$|\mathcal{M}(k; p_1, p_2, p_3)|^2 \simeq g_s^2 \mu^{2\epsilon} 2 \Big((T_3^2 - T_1^2 - T_2^2)\mathcal{S}_{12}(k) + (T_2^2 - T_1^2 - T_3^2)\mathcal{S}_{13}(k) + (T_1^2 - T_2^2 - T_3^2)\mathcal{S}_{23}(k) \Big) |\mathcal{M}(p_1, p_2, p_3)|^2. \tag{35}$$

2.3 Coloured partons in the initial state

As we briefly pointed out at the beginning of this chapter, the soft and collinear divergences cancel out provided that the production cross section is defined inclusively, i.e. the final state F is produced, where F is an ensemble of jets and/or heavy particles,

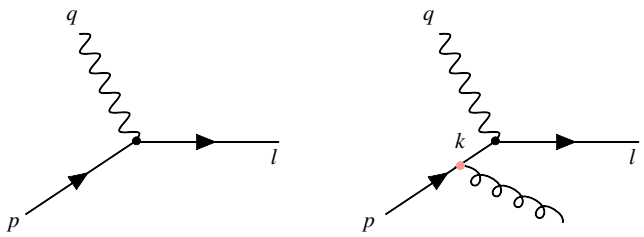

Figure 4: Amplitudes for virtual photon scattering off a quark

but allowing for the production of additional radiation X.
This is a general property of the scattering of non coloured partons, so leptons or photons. If the scattering involves coloured particles in the initial state, the IR divergences in the final state still cancel for inclusive observables. However, mass singularities associated with collinear emission in the initial state do not cancel out and require separate treatment.
To better illustrate how collinear divergences in the initial state are treated in scattering processes with coloured partons in the initial state, we consider the scattering of a virtual photon off a "free" (i.e. independent of being inside a proton) quark with momentum p (see ref [23]) as showed on the left hand side of Figure (4).

$$\gamma^*(q) + q(p) \to q(l) \tag{36}$$

At lowest order in QCD, the virtual photon sees a point-like quark; hence the "free" quark distribution function is given by

$$q^{(0)}_{\text{free}}(x) = \delta(1-x). \tag{37}$$

Higher order corrections generate a colour field surrounding the quark. Note that for the rest of this section we will use the lower indices "free" and "proton" to denote a quark independent of its life in the proton and a quark in the proton, respectively.
Next we consider the order α_s correction to the "free" quark distribution coming from the collinear emission of a gluon from the initial state quark as shown on the right hand side of figure (4).
This correction together with the leading order contribution gives

$$q_{\text{free}}(x) = \delta(1-x) + \frac{\alpha_s}{\pi}\left(\langle \hat{P}_{qq}(x)\rangle \log\left(\frac{Q^2}{\Lambda^2}\right) + C(x)\right) \tag{38}$$

where $\langle \hat{P}_{qq}(x)\rangle$ is the azimuthally averaged, unregularized AP splitting function obtained from equation (16) for $d = 4$ and $C(x)$ is a calculable function. The important thing to note here is the collinear divergence associated to the limit in which the gluon is emitted collinearly to the quark. It is exposed as a logarithmic enhancement in the cut-off Λ on the gluon transverse momentum.
This is not quite the complete answer for q_{free}. The full result requires the inclusion of virtual gluon radiation as well. A physical argument that provides a useful short-cut to

this computation is to note that because the delta function $\delta((p+q)^2)$ is common to all the virtual diagrams, their contribution to the quark distribution is proportional to $\delta(1-x)$. Thus, for example, the splitting function becomes

$$\langle \hat{P}_{qq}(x) \rangle \to \langle \hat{P}_{qq}(x) \rangle + A\delta(1-x). \tag{39}$$

Second, in order to conserve quark (i.e. Baryon) number, the integral of the quark distribution cannot vary with Q^2. This implies that the function on the right hand side of Eq. (38) must integrate to 0. We can use this condition to fix the coefficient A. The final answer is the same as before with the unregularised splitting kernel replaced by the regularised one:

$$\langle P_{qq}(x) \rangle = \frac{C_F}{2}\left[\frac{1+x^2}{(1-x)_+} + \frac{3}{2}\delta(1-x)\right]. \tag{40}$$

Note that we have introduced the "plus" distribution prescription in order to regulate the soft divergence at $x \to 1$.
We therefore have

$$q_{\text{free}}(x, Q^2) = \delta(1-x) + \frac{\alpha_s}{\pi}\left(\langle P_{qq}(x) \rangle \log\left(\frac{Q^2}{\Lambda^2}\right) + C(x)\right). \tag{41}$$

At variance to the previous section, this collinear divergence is not subject to the theorems of cancellation of singularities since the underlying hard-scattering process $\gamma^* + q \to q + X$ probes the quark density at scales given by the virtuality of the photon and is not completely inclusive over the initial state.
The situation is even more severe when considering the realistic case of a quark inside the proton. In fact, in order to obtain the quark distribution inside the proton, we need to convolute Eq. (41) with the probability density function $q_0(x)$ of finding a quark in the proton and also take into account that the quark carries in general a fraction ξ of the proton's total momentum. This gives

$$q_{\text{proton}}(x, Q^2) = q_0(x) + \frac{\alpha_s}{\pi}\int_x^1 \frac{d\xi}{\xi} q_0(\xi)\left\{\langle P_{qq}\left(\frac{x}{\xi}\right)\rangle \log\left(\frac{Q^2}{\Lambda^2}\right) + C\left(\frac{x}{\xi}\right)\right\}. \tag{42}$$

Analogously to the renormalisation of the coupling constant, we can regard $q_0(x)$ as a bare, non measurable, quantity. The collinear singularities are absorbed into this bare distribution at a "factorisation scale" μ.
In other words, we define a "renormalised" distribution $q_{\text{proton}}(x, \mu^2)$ by

$$q_{\text{proton}}(x, \mu^2) = q_0(x) + \frac{\alpha_s}{\pi}\int_x^1 \frac{d\xi}{\xi} q_0(\xi)\left\{\langle P_{qq}\left(\frac{x}{\xi}\right)\rangle \log\left(\frac{\mu^2}{\Lambda^2}\right) + C\left(\frac{x}{\xi}\right)\right\}, \tag{43}$$

and then rexpress the bare distribution in terms of the renormalised as

$$q_0(x) = q_{\text{proton}}(x, \mu^2) - \frac{\alpha_s}{\pi}\int_x^1 \frac{d\xi}{\xi} q_{\text{proton}}(\xi, \mu^2)\left\{\langle P_{qq}\left(\frac{x}{\xi}\right)\rangle \log\left(\frac{\mu^2}{\Lambda^2}\right) + C\left(\frac{x}{\xi}\right)\right\}. \tag{44}$$

This gives

$$q_{\text{proton}}(x, Q^2) = q_{\text{proton}}(x, \mu^2) + \frac{\alpha_s}{\pi} \int_x^1 \frac{d\xi}{\xi} q_{\text{proton}}(\xi, \mu^2) \left\{ \langle P_{qq} \left(\frac{x}{\xi} \right) \rangle \log \left(\frac{Q^2}{\mu^2} \right) + \ldots \right\}, \tag{45}$$

and is finite. In equation (45), the ellipses stand for the finite (non-logarithmic) contributions. It is interesting to note that in this procedure of absorbing the logarithmic singularities in the bare distribution, there is still arbitrariness in how the finite contributions are treated. How much finite contribution is factored out (i.e. absorbed in the bare distribution) is what defines the so-called "factorisation scheme". In particular, in this thesis, all calculations are done in the $\overline{MS}$ scheme, where in addition to the divergent contribution, only a ubiquitous $\log(4\pi) - \gamma_E$ contribution is absorbed into the bare distribution.

3 q_T subtraction method

At the beginning of the previous chapter we briefly illustrated the appearance of infrared divergences in real radiation corrections. In particular, we have seen that these divergences appear only after integrating on the phase space of the emitted partons, in contrast to the explicit structure of the poles in ϵ in virtual corrections. The easiest way to make the cancellation between real and virtual corrections manifest is to integrate over the entire phase space of the real parton emitted. In doing so, however, kinematic information about the process is lost. To see this, consider again the process $e^+e^- \to$ hadrons at NLO, which was discussed in Chapter (2). For this particular example, integration over the entire phase space of the emitted real gluon would lead to the full NLO cross section

$$\sigma_{\text{tot}} = \sigma_{2-\text{jet}} + \sigma_{3-\text{jet}} \, . \tag{46}$$

One would thus lose kinematic information about the 2-jet and 3-jet processes, which could in principle be measured at an e^+e^- collider. This motivates the introduction of a so-called subtraction scheme, a method that allows to extract the singularities of the real correction without having to integrate over the entire phase space of the radiated parton.
Roughly speaking, subtraction procedures can be divided into two categories

- Local subtraction method,
- Slicing methods.

The basic idea of local subtraction methods (see e.g. [24], [25] and [26]) is to identify a function S that reproduces the matrix elements in the unresolved (IR singular) limits and is simple enough to be integrated over the unresolved phase space. This function can then be subtracted from the real correction to make it finite, and added back to the virtual correction to cancel the infrared poles. The discussion of this type of subtraction methods is beyond the scope of this thesis and will not be discussed further.
In this thesis, for the computation of NLO cross sections, we make use of the q_T-subtraction method (see Ref. [11]). This method can be classified as a slicing method. The basic idea of q_T-subtraction is to identify an observable, q_T, that represents a **good resolution variable** in the sense that

- for $q_T > 0$ the real emission cross section cannot be divergent. The real corrections are then finite and they have the IR structure of a LO + jet computation.
- All the IR divergences are contained in the small q_T limit.

One can then use this observable to slice up the phase space into an unresolved part and a resolved part. This can be schematically written as

$$\int d\Phi \int_0^{q_T^{\max}} |\mathcal{M}_R|^2 \mathcal{F} dq_T = \int d\Phi \left(\int_0^{q_T^{\text{cut}}} |\mathcal{M}_R|^2 \mathcal{F} dq_T + \int_{q_T^{\text{cut}}}^{q_T^{\max}} |\mathcal{M}_R|^2 \mathcal{F} dq_T \right) , \tag{47}$$

where $d\Phi$ represents the additional variables on which the real phase space depends and $\mathcal{F}$ is a general measurement function.
The slicing in q_T on the r.h.s. of the above equation allows us to identify the integral for $0 < q_T < q_T^{\rm cut}$ with all the Born-like soft-collinear contributions and the integral for $q_T > q_T^{\rm cut}$ with the finite LO+jet contribution.
For a generic massive non coloured final state F, one can write the q_T-subtraction formula schematically as

$$d\sigma^F_{\rm NLO} = \mathcal{H}^F_{\rm NLO} \otimes d\sigma^F_{\rm LO} + \lim_{q_T/Q\to 0}\left[d\sigma^{F+jet}_{\rm LO} - d\sigma^{\rm CT}_{\rm NLO}\right], \tag{48}$$

In particular the first term on the right hand side of the above equation represents all the contributions that live at $q_T = 0$ while the second term represents the subtracted real corrections.
To illustrate each piece of the q_T subtraction formula in further detail we consider the explicit example of Higgs production at NLO.

3.1 Setup of the calculation

The SM Higgs boson does not couple directly to gluons (or photons), while it couples to quarks via a Yukawa interaction proportional to the quark mass. Hence in QCD with $n_f = 5$ light flavours, Higgs production in gluon fusion is mediated trough a heavy top quark loop. If all scales involved in the process under consideration are substanstially smaller then the top quark mass, it is possible to integrate out the top quark loop by taking the limit $m_t \to \infty$. The resulting effective field theory (EFT) lagrangian consists of five-flavour QCD and a term coupling the Higgs field to the square of the gluon field strength tensor,

$$\mathcal{L}_{\rm eff} = -\frac{1}{4} A H G^a_{\mu\nu} G^{a,\mu\nu}. \tag{49}$$

The effective coupling A is given by

$$A = \frac{\alpha_s}{3\pi v} + \mathcal{O}(\alpha_s^2), \tag{50}$$

where v is the vacuum expectation value parameter, $v^2 = (G_F\sqrt{2})^{-1}$.
The effective Lagrangian generates three interaction vertices depicted in the figure(5) with the corresponding Feynman rules. The two-gluon-Higgs-boson vertex is proportional to the tensor

$$H^{\mu\nu}(p_1, p_2) = g^{\mu\nu} p_1 \cdot p_2 - p_1^\nu p_2^\mu \,, \tag{51}$$

while the vertices involving three and four gluons and the Higgs boson are exactly proportional to their counterpart from pure QCD

$$V^{\mu\nu\rho}(p_1, p_2, p_3) = (p_1 - p_2)^\rho g^{\mu\nu} + (p_2 - p_3)^\mu g^{\nu\rho} + (p_3 - p_1)^\nu g^{\rho\mu} \,, \tag{52}$$

and

$$\begin{aligned} X^{\mu\nu\rho\sigma}_{abcd} &= f_{abe} f_{cde} (g^{\mu\rho} g^{\nu\sigma} - g^{\mu\sigma} g^{\nu\rho}) + f_{ace} f_{bde} (g^{\mu\nu} g^{\rho\sigma} - g^{\mu\sigma} g^{\nu\rho}) \\ &\quad + f_{ade} f_{bce} (g^{\mu\nu} g^{\rho\sigma} - g^{\mu\rho} g^{\nu\sigma}) \,. \end{aligned} \tag{53}$$

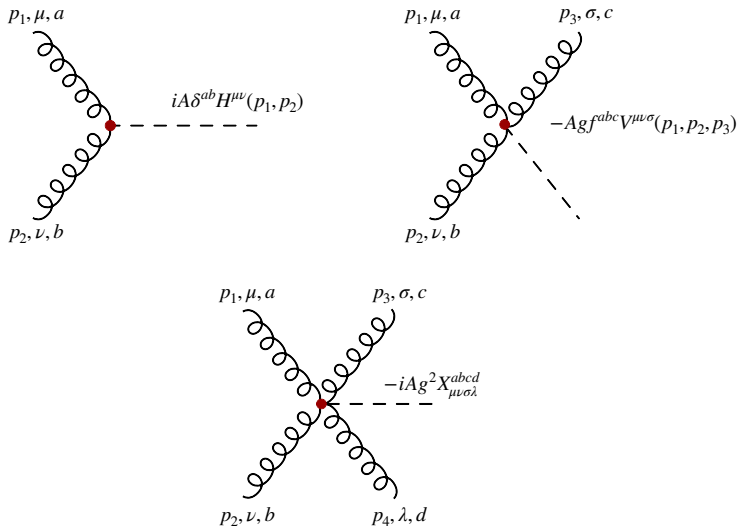

Figure 5: Interaction vertices in HEFT

3.2 Higgs production at NLO

We look at inclusive Higgs production in gluon gluon fusion[2]

$$g(p_1) + g(p_2) \to H(p) + X(k) \tag{54}$$

where p_1, p_2 are the momenta of the incoming gluons, p is the momentum of the Higgs and k is the momentum of the additional radiation.
We start discussing the needed counterterm within the q_T-subtraction formalism. For this we need to consider the real corrections, where one parton recoils against the Higgs. For Higgs production at NLO, in the gg-channel, the extra parton is always a gluon as showed in Figure (6) . The kinematics of the process in equation (54) can be worked out in terms of the usual Mandelstam invariants

$$s = (p_1 + p_2)^2,\ t = (p_1 - p)^2,\ u = (p_2 - p)^2 \text{ and } z = \frac{m_H^2}{s}\ , \tag{55}$$

and with $q_T = \frac{tu}{s}$ the transverse momentum of the Higgs. We denote the corresponding matrix element as $\mathcal{M}_{gg\to hg}(p_1, p_2, p, k)$.
We observe that, when q_T is small, the additional gluon is constrained to be either collinear to one of the incoming partons or soft. Thus the $q_T \to 0$ limit contains the three possible singular regions of the $\mathcal{M}_{gg\to hg}$ matrix element:

- first collinear region: $p_1 \cdot k \to 0$;
- second collinear region: $p_2 \cdot k \to 0$;

[2]At NLO, two other channels (qg and $q\bar{q}$) have to be considered. However, to illustrate the general idea of q_T-subtraction, we restrict ourselves to the gg-channel only.

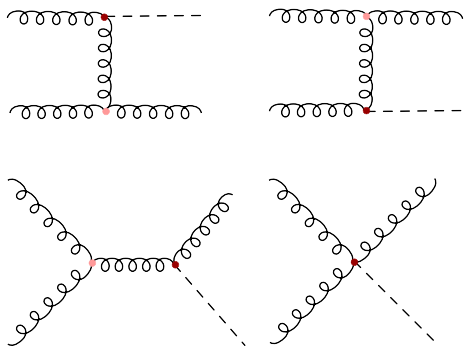

Figure 6: All Feynman diagrams contributing to the real correction at NLO in HEFT

- soft region: $k^\mu \to 0$.

As shown in Ref. [27], it is possible to capture all singular limits by a single "collinear" factorisation formula

$$\lim_{q_T\to 0} |\mathcal{M}_{gg\to Hg}|^2 \simeq \frac{8\pi\alpha_s\mu^{2\epsilon}}{zp_1\cdot k}\langle \hat{P}_{gg}(z)\rangle |\mathcal{M}_{gg\to H}(zp_1,p_2,p)|^2 + (1\leftrightarrow 2). \tag{56}$$

as a result of colour-coherence. The counterterm can be therefore written as

$$\begin{aligned}\sigma^{\rm CT}_{gg\to Hg} &= \int_{\tau_0}^1 dx_1 \int_{\tau_0/x_1}^1 dx_2 f_g(x_1) f_g(x_2) \int d\Phi_2^d(k,p) \lim_{q_T\to 0} \frac{|\mathcal{M}_{gg\to Hg}|^2}{2\hat{s}}\Theta(q_T - q_T^{\rm cut}) \qquad (57)\\ &= \frac{\alpha_s}{\pi}\left(\frac{4\pi^2\mu^2}{m_H^2}\right)^\epsilon \int_{\tau_0}^1 dx_1 \int_{\tau_0/x_1}^1 dx_2 f_g(x_1) f_g(x_2) \frac{1}{2\hat{s}} \int d\Omega_{d-2} \int_0^{(x_T^{\rm max})^2} \frac{dx_T^2}{x_T^2}(x_T^2)^{-\epsilon} \\ &\times \frac{(1-z)}{m_H^2\sqrt{(1-z)^2-4zx_T^2}} \langle \hat{P}_{gg}(z)\rangle |\mathcal{M}_{gg\to H}(zp_1,p_2,p)|^2 + (x_1\leftrightarrow x_2)\,, \qquad (58)\end{aligned}$$

where in the last step we substituded the explicit formula for the two body phase space (see Appendix A) and used

$$\int_{-1}^1 d\cos\theta(\delta^+ + \delta^-)\frac{1}{p_1\cdot k} = \frac{2(1-z)}{m_H^2 x_T^2}. \tag{59}$$

Next we perform the change of variables

$$(x_1,x_2)\to(\tilde{x}_1,\tilde{x}_2) \;\text{ with }\; \tilde{x}_1 = zx_1 \;\text{ and }\; \tilde{x}_2 = x_2 \tag{60}$$

and then again

$$(\tilde{x}_1,\tilde{x}_2)\to(\tau,y) \;\text{ with }\; \tau = \tilde{x}_1\tilde{x}_2 \;\text{ and }\; y = \frac{1}{2}\log\left(\frac{\tilde{x}_1}{\tilde{x}_2}\right). \tag{61}$$

Moreover we can insert

$$1 = \int dz\delta(1-z) = \int dz\tau\delta(\tau - \frac{m_H^2}{S}), \tag{62}$$

and get

$$\begin{aligned}
&\frac{\alpha_s}{\pi}\frac{\left(\frac{4\pi\mu^2}{m_H^2}\right)^\epsilon}{\Gamma[1-\epsilon]}\int_{\ln\sqrt{\tau_0}}^{-\ln\sqrt{\tau_0}} dy f_g(\tilde{x}_2)\hat{\sigma}^{(0)}_{gg\to H}\int_0^{(x_T^{\max})^2}\frac{dx_T^2}{x_T^2}(x_T^2)^{-\epsilon}\\
&\times\int_{\tilde{x}_1}^{z_{\max}}\frac{dz}{z}\frac{1-z}{\sqrt{(1-z)^2-4zx_T^2}}\langle\hat{P}_{gg}(z)\rangle f_g\left(\frac{\tilde{x}_1}{z}\right) + (x_1\leftrightarrow x_2)\,,
\end{aligned} \tag{63}$$

with $\tau_0 = \frac{m_H^2}{S_{\text{had}}}$. The limits of z are given by the kinematics. In particular, since we are interested in the small q_T limit, we can approximate

$$z_{\max} \approx 1 - 2x_T.$$

The integral over the threshold variable z can then be written as

$$\begin{aligned}
&\int_{\tilde{x}_1}^{1-2x_T}\frac{dz}{z}\frac{1-z}{\sqrt{(1-z)^2-4zx_T^2}}\langle\hat{P}_{gg}(z)\rangle f_g\left(\frac{\tilde{x}_1}{z}\right)\\
&= \int_{\tilde{x}_1}^{1-2x_T}\frac{dz}{z}\frac{(1-z)\langle\hat{P}_{gg}(z)\rangle f_g(\frac{\tilde{x}_1}{z}) - zC_A f_g(\tilde{x}_1)}{\sqrt{(1-z)^2-4zx_T^2}}
\end{aligned} \tag{64}$$

$$+\, C_A f_g(\tilde{x}_1)\int_{\tilde{x}_1}^{1-2x_T} dz\frac{1}{\sqrt{(1-z)^2-4zx_T^2}}. \tag{65}$$

The integral in equation (64) is finite for every x_T thus, if we are only interested in the small q_T limit, we can simply set $x_T = 0$. This gives

$$\int_{\tilde{x}_1}^1\frac{dz}{z}\frac{(1-z)\langle\hat{P}_{gg}(z)\rangle f_g(\frac{\tilde{x}_1}{z}) - zC_A f_g(\tilde{x}_1)}{1-z} \tag{66}$$

$$= \int_{\tilde{x}_1}^1\frac{dz}{z}\langle P_{gg}(z)\rangle f_g(\frac{\tilde{x}_1}{z}) - C_A f_g(\tilde{x}_1)\log(1-\tilde{x}_1) - \frac{(11C_A-2n_f)}{12}f_g(\tilde{x}_1)\,, \tag{67}$$

with the regularised splitting function

$$\langle P_{gg}(z)\rangle = C_A\left[\frac{z}{(1-z)_+} + \frac{1-z}{z} + z(1-z)\right] + \frac{1}{2}\delta(1-z)\frac{(11C_A-2n_f)}{12}. \tag{68}$$

The integral in equation (65) can be evaluated explicitly and then expanded for small x_T

$$C_A f_g(x_1)\int_{x_1}^{1-2x_T} dz\frac{1}{\sqrt{(1-z)^2-4zx_T^2}} \approx C_A f_g(x_1)(\log(1-x_1) - \log(x_T)). \tag{69}$$

The updated counterterm reads

$$\frac{\alpha_s}{\pi}\frac{\left(\frac{4\pi\mu^2}{m_H^2}\right)^\epsilon}{\Gamma[1-\epsilon]}\int_{\ln\sqrt{\tau_0}}^{-\ln\sqrt{\tau_0}} dy f_g(\tilde{x}_2)\hat{\sigma}^{(0)}_{gg\to H}\int_0^{(x_T^{\max})^2}\frac{dx_T^2}{x_T^2}(x_T^2)^{-\epsilon}$$
$$\times\left\{\int_{\tilde{x}_1}^1\frac{dz}{z}\langle P_{gg}(z)\rangle f_g\left(\frac{\tilde{x}_1}{z}\right)-\frac{(11C_A-2n_f)}{12}f_g(\tilde{x}_1)-C_A\log(x_T)f_g(\tilde{x}_1)\right\}$$
$$+(\tilde{x}_1\leftrightarrow\tilde{x}_2). \tag{70}$$

This is almost the final form of the counterterm, the only thing we still need to take care of is the integration over x_T. In particular, having already identified x_T as a good resolution variable, we can apply the slicing method discussed above and write

$$\int_0^{(x_T^{\max})^2}\frac{dx_T^2}{x_T^2}(x_T^2)^{-\epsilon}\left\{A+\frac{B}{2}\log(x_T^2)\right\}$$
$$=\left(\int_0^{r_{\text{cut}}^2}dx_T^2+\int_{r_{\text{cut}}^2}^{(x_T^{\max})^2}dx_T^2\right)\frac{(x_T^2)^{-\epsilon}}{x_T^2}\left\{A+\frac{B}{2}\log(x_T^2)\right\}, \tag{71}$$

where A and B represent the terms in the second line of equation (70). The first integral on the second line of the above equation represents the Born-like soft-collinear approximation (see equation (47)), therefore, for the computation of the counterterm we only have to focus on this piece:

$$\int_0^{r_{\text{cut}}^2}dx_T^2(x_T^2)^{-1-\epsilon}\left\{A+\frac{B}{2}\log(x_T^2)\right\}$$
$$=-\left(\frac{A}{\epsilon}+\frac{B}{2\epsilon^2}\right)+\left(A\log(r_{\text{cut}}^2)+\frac{B}{4}\log^2(r_{\text{cut}}^2)\right)+\mathcal{O}(\epsilon)\,. \tag{72}$$

From the above computation we get the divergent $r_{\text{cut}}=0$ contribution, regulated by the poles in ϵ. This piece contributes to the $\mathcal{H}$-function in equation (48) as

$$\lim_{r_{\text{cut}}\to 0}\sigma^{gg}_{CT}=\frac{\alpha_s}{\pi}\frac{\left(\frac{4\pi\mu^2}{m_H^2}\right)^\epsilon}{\Gamma[1-\epsilon]}\int_{\ln\sqrt{\tau_0}}^{-\ln\sqrt{\tau_0}}dy\;\hat{\sigma}^{(0)}_{gg\to H}\left\{f_g(\tilde{x}_1)f_g(\tilde{x}_2)\right.$$
$$\left.\times\left[\frac{C_A}{2\epsilon^2}-\frac{(11C_A-2n_f)}{12}\frac{1}{\epsilon}\right]-f_g(\tilde{x}_1)(f_g\otimes\langle P_{gg}\rangle)(\tilde{x}_2)\frac{1}{\epsilon}\right\}$$
$$+(\tilde{x}_1\leftrightarrow\tilde{x}_2)\,, \tag{73}$$

with the short hand notation $(f_g\otimes\langle P_{gg}\rangle)(\tilde{x}_2)$ for the convolution of the AP splitting function with the gluon pdf.

It is important to note that the ϵ^2 pole and the ϵ pole multiplying the pieces defined at $z=1$ cancel when combined with the IR poles of the virtual as expected from the KLN theorem.

However, the purely initial state collinear pole, i.e. the one that multiplies the convolution of the splitting function, does not cancel with the poles of the virtual. As already

mentioned in the section (2), this pole is included in the definition of the renormalised parton distribution function by applying $\overline{MS}$ subtraction.
The other contribution from equation (72) is the one at $r_{\rm cut} \neq 0$. In particular, this piece is used to subtract the divergence of the real in $d = 4$ dimensions. We can therefore write the q_T subtraction counterterm as

$$\sigma^{gg}_{CT} = \frac{\alpha_s}{\pi}\int_{\ln\sqrt{\tau_0}}^{-\ln\sqrt{\tau_0}} dy\ \hat{\sigma}^{(0)}_{gg\to H}\Bigg\{\frac{1}{4}C_A f_g(x_1)f_g(x_2)\tilde{L}_2(r_{cut}) + \Bigg[-\frac{(11C_A - 2n_f)}{12}f_g(x_1)f_g(x_2) + f_g(x_1)(f_g \otimes \langle P_{gg}\rangle)(x_2)\Bigg]\tilde{L}_1(r_{cut})\Bigg\} + (x_1 \leftrightarrow x_2)\ , \tag{74}$$

with

$$\tilde{L}_1(r_{cut}) \equiv \log\left(\frac{1}{r^2_{cut}}\right)\ , \tag{75}$$

$$\tilde{L}_2(r_{cut}) \equiv \log^2\left(\frac{1}{r^2_{cut}}\right)\ , \tag{76}$$

and the partonic level born cross section (in $d = 4$) given by

$$\hat{\sigma}^{(0)}_{gg\to H} = \frac{\alpha_s^2}{\pi}\frac{m_H^2}{576v^2 S}. \tag{77}$$

To complete the NLO calculation, we need to consider the contributions that live at $q_T = 0$, i.e. the parts that enter the $\mathcal{H}$ function (see 48). In the following we list and explain all these contributions.
The Born cross section (σ_B) is clearly defined at $q_T = 0$ since at this order, in perturbation theory, the Higgs is produced with no accompayining radiation.
The virtual correction to the LO process is given by the 1-loop amplitude interfered with the lowest order one. The IR singular structure of the virtual correction is universal and can be found in equation (38) of Ref. [27]. In particular, once the IR singularities are subtracted trough a subtraction operator

$$\tilde{I}_{gg\to H} = -\frac{1}{4}\left(\frac{M^2}{\mu_R^2}\right)^{-\epsilon}\left\{\left(\frac{1}{\epsilon^2} + i\pi\frac{1}{\epsilon} - \frac{\pi^2}{12}\right)2C_A + \frac{2}{\epsilon}\frac{(11C_A - 2n_f)}{12}\right\} \tag{78}$$

one gets a finite contribution (the subtracted virtual) $|\tilde{\mathcal{M}}^{(1)}_{gg\to H}|^2$, with

$$\tilde{\mathcal{M}}^{(1)}_{gg\to H} = [1 - \tilde{I}_{gg\to H}]\mathcal{M}^{(1)}_{gg\to H}. \tag{79}$$

Note in particular that the subtraction operator could in principle be read off the $z = 1$ piece of the integrated counterterm in equation (73).
There are two contributions coming from the $\overline{MS}$ subtraction. One is due to the fact, that only contributions below a factorisation scale μ_F^2 are subtracted. This contribution can be represented in direct space as

$$\sigma_B \otimes \frac{\alpha_s}{\pi}P_{gg}(z)\log\left(\frac{Q^2}{\mu_F^2}\right)\ . \tag{80}$$

The other contribution comes from choosing a specific subtraction scheme, in particular for the "hard scheme" defined in Ref. [28] this is given by the so called beam functions $C_{ab}(z)$ and is zero for the specific case of gluon gluon splitting, i.e., $C_{gg}(z) = 0$.
All in all we can write the full $q_T = 0$ contribution in direct space as

$$\sigma_B \otimes \left(1 + \frac{\alpha_s}{\pi} H_g^{H(1)} - \frac{\alpha_s}{\pi} k\beta_0 \log\left(\frac{Q^2}{\mu_R^2}\right) + \frac{\alpha_s}{\pi} \log\left(\frac{Q^2}{\mu_F^2}\right)(P_{gg}(z_1) + P_{gg}(z_2))\right), \quad (81)$$

where $H_g^{H(1)}$ is the ratio of the subtracted virtual matrix element squared and the Born matrix element squared and is defined at $\mu_R^2 = Q^2$

$$H_g^{H(1)} = \frac{|\tilde{\mathcal{M}}^{(1)}_{gg\to H}(\alpha_s(Q^2))|^2}{|\mathcal{M}^{(0)}_{gg\to H}(\alpha_s(Q^2))|^2}. \quad (82)$$

In particular $H_g^{H(1)} = C_A \frac{\pi^2}{2} + \frac{11}{2}$ and can be found in eq. (85) of Ref. [28].
The factor $\frac{\alpha_s}{\pi} k\beta_0 \log\left(\frac{Q^2}{\mu_R^2}\right)$ (k are the powers of α_s at LO, i.e., $k = 2$ for our case) comes from the running of the coupling and is needed to counterbalance the change of scale when setting $\mu_R = Q$ in $H_g^{H(1)}$.

3.2.1 Results

All the graphs shown in this section were generated via the code `higgs_at_nlo` implemented by us and publicly available at:
`https://gitlab.com/mark.costantini/h_jet_nlo`.
In figure (7) we show the r_{cut} dependence of the NLO cross section for $gg \to H + X$, at 13TeV and for different scales μ_F and μ_R. Note that the results are normalised to the r_{cut} independent NLO cross section obtained by `MCFM` (which implements the dipole subtraction method, see Ref. [24, 25]). In particular, in the plotted range, we observe a flat r_{cut} dependence. This is because the power suppressed contributions, left after the cancellation of the logarithmic singularities at small r_{cut}, are quadratic (and thus suppressed in the plotted range) for the inclusive production of a colourless final state [29]. In the following table we compare the $r_{\text{cut}} = 0$ extrapolated result of q_T subtraction against the `MCFM` result for the 3 different scale variations. We find an agreement whitin a few sigmas. Moreover, by comparing these results with the LO results we observe a K factor of approximately $K \approx 2.3$.

NLO [pb]	$\mu_F = \mu_R = m_H$	$\mu_F = \frac{m_H}{2}, \mu_R = 2m_H$	$\mu_F = 2m_H, \mu_R = \frac{m_H}{2}$
q_T subtraction	30.749 ± 0.003	24.341 ± 0.002	39.310 ± 0.004
`mcfm`	30.741 ± 0.001	24.343 ± 0.003	39.328 ± 0.004
LO [pb]	13.322 ± 0.002	10.431 ± 0.001	17.034 ± 0.002

In figure (8) we plot the NLO differential distribution for the Higgs rapidity obtained with our numerical program against that calculated with `MCFM`, and find excellent agreement. Moreover, comparing the NLO distribution with the LO distribution we still observe a K factor of about 2.3.

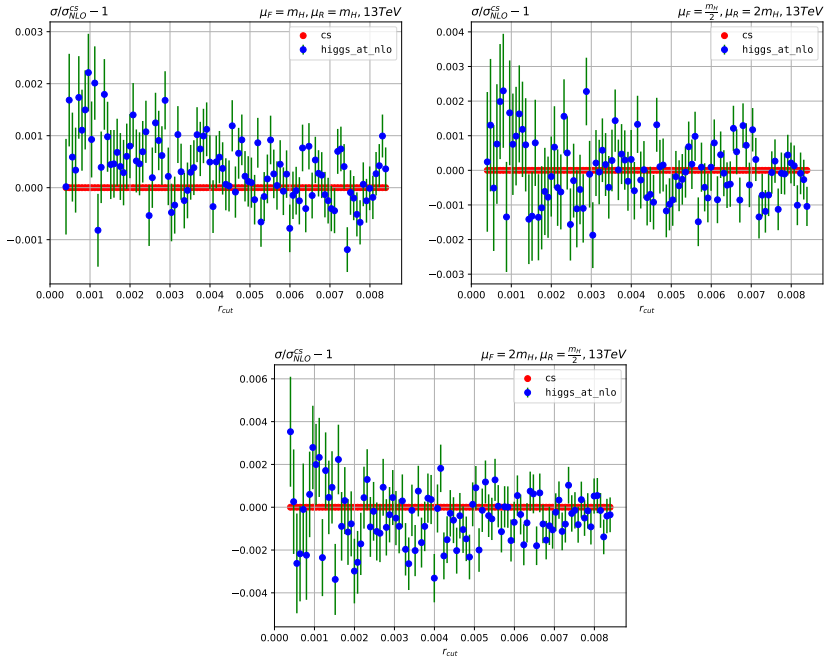

Figure 7: Dependence of the NLO $gg \to H + X$ cross section on r_{cut}. The results are normalised to the r_{cut} - independent NLO cross section computed with MCFM

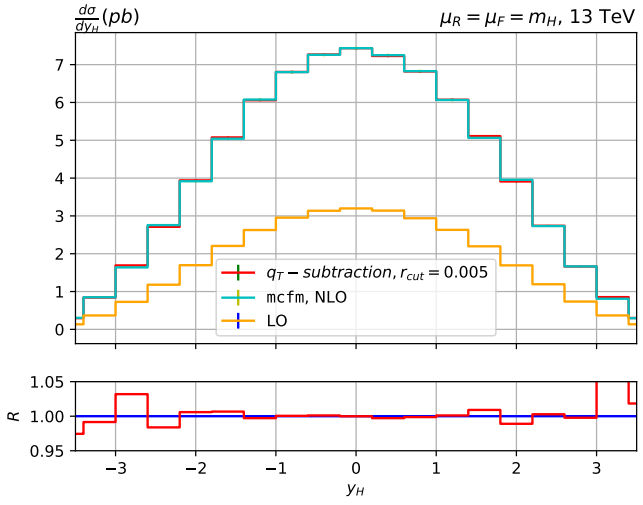

Figure 8: Rapidity distribution of the Higgs at the LHC (at 13TeV) computed at NLO accuracy. Comparison of our results (in red) with the MCFM results (in cyan). In orange the LO distribution.

4 Higgs plus Jet production at NLO

We consider the inclusive production of a Higgs boson together with a high transverse momentum jet in proton proton collisions,

$$p(P_1) + p(P_2) \to H(p_3) + j(p_4) + X. \tag{83}$$

The LO cross section for Higgs production at non-vanishing transverse momentum is at $\mathcal{O}(\alpha_s^3)$ and receives contributions from the parton level processes $gg \to Hg$, $q(\overline{q})g \to Hq(\overline{q})$ and $q\overline{q} \to Hg$, with the first two accounting for the bulk of the cross section. The relevant contributions at NLO are listed in the following table.

LO	$gg \to Hg$	$qg \to Hq$	$q\overline{q} \to Hg$
NLO	$gg \to Hgg$	$gg \to Hq\overline{q}$	$qg \to Hqg$
	$qq \to Hqq$	$q\overline{q} \to Hgg$	$q\overline{q} \to Hq\overline{q}$

To calculate the NLO cross section, we use the q_T subtraction method. As mentioned in the previous section, the basic idea of the q_T-subtraction method is to identify an observable that is sensitive to IR radiation and that is related to the transverse momentum of the initial-state radiation. For the case of the production of a massive colour singlet, such as the Higgs, we have seen (see section (3.2)) that the correct observable is the transverse momentum of the colour singlet itself. However, this is no longer correct if one has an additional coloured parton in the final state. In the following, we will first discuss the correct identification of the q_T subtraction observable for a process with jets in the final state, then the calculation of the q_T counterterm, with special attention to the main differences to the colour singlet case, and finally the calculation of the contribution that lives at $q_T = 0$.

4.1 q_T imbalance and clustering algorithm

A first natural guess for $\mathbf{q_T}$ could be

$$\mathbf{q_T} = \mathbf{p_T}^{\text{Higgs}} + \mathbf{p_T}^{\text{Hardest Parton}}\ , \tag{84}$$

i.e. one identifies the hardest parton as the jet at parton level. In fact, it is clear that for all processes with Born-like kinematics, $\mathbf{q_T}$ is exactly zero, since the parton and the Higgs are back-to-back in this configuration. However, special care must be taken when there are two partons in the final state. In particular, in the limits in which the radiation is either soft or collinear, the $\mathbf{q_T}$ observable defined above is vanishing, as it should be. Nonetheless, configurations characterised by the presence of two hard and collinear final state partons have a non-vanishing $\mathbf{q_T}$ despite being divergent. We conclude that the definition of $\mathbf{q_T}$ given in Eq. (84) does not regularise the final state collinear singularity. We can modify it by defining the jet only after applying a clustering algorithm. To do so let us define the kinematics of the process pre-clustering[3] as

$$a(p_1) + b(p_2) \to H(p_3) + c(p_4) + d(p_5), \tag{85}$$

[3] this kinematical variables are to be contrasted with the ones defined post-clustering

with a, b, c and d generic coloured partons. Given the three final state momenta (p_3, p_4 and p_5) and the two clustering parameters R_0 (see section (2.1.1)) and $p_T^{\text{min,jet}}$, the clustering algorithm works as follows.

1. Check wheter the two partons cluster into a single jet, i.e. compute $R_{4,5}$[4] as

$$R_{4,5}^2 = 2(\cosh(y_4 - y_5) - \cos(\phi_4 - \phi_5)) \tag{86}$$

   `if` $R_{4,5} < R_0 \rightarrow$ the two partons are clustered together.
   The resulting event represents a Higgs and a jet perfectly balanced and, hence, $\mathbf{q_T} = 0$. In particular, two collinear partons in the final state will be clustered together, solving the final-state radiation (FSR) issue.

2. Check if the leading jet passes the cut

   `if` $p_T(p_{\text{jet}}) < p_T^{\text{min,jet}} \rightarrow$ cut the event .

3. Finally apply the cut on the q_T of the Higgs plus jet system

   `if` $q_T < q_T^{\text{cut}} \rightarrow$ cut the event .

The new, post-clustering, kinematics now reads as follows

$$a(p_1) + b(p_2) \rightarrow H(p_3) + j(p_{\text{jet}}) + X(k), \tag{87}$$

with

$$\mathbf{q_T} = \mathbf{p_T}^{\text{Higgs}} + \mathbf{p_T}^{\text{hardest jet}}, \tag{88}$$

and the invariants

$$\begin{aligned} &Q^2 = (p_3 + p_{\text{jet}})^2,\ s = (p_1 + p_2)^2,\ t = (p_1 - p_{\text{jet}})^2, \\ &u = (p_2 - p_{\text{jet}})^2,\ z = \frac{Q^2}{s}. \end{aligned} \tag{89}$$

Note in particular that k in (87) represents the additional softer radiation.
In this way $\mathbf{q_T}$ represents a good resolution variable since sensitive to IR radiation.
Before presenting the explicit form of the counterterm and $\mathcal{H}$-function, we briefly discuss the relevant contributions to Higgs plus jet production in the collinear/soft regions of the 3-particle phase space. This will be of help in understanding the various pieces that enter in the calculation.
In figure (9) we show in a schematical way all the relevant configurations. Diagrams 1 and 2 represent the final state splitting of a generic parton into two hard collinear partons or into a collinear pair of hard parton and soft gluon. These two configurations are clustered into a single jet (see step 1 of the clustering algorithm) and thus provide a Born-like contribution to the process, which can be written as follows

$$\sigma^{\text{jet}} = \sigma_B \otimes \mathcal{J}. \tag{90}$$

[4] Note that this radius definition differs from the standard $R^2 = (\Delta y)^2 + (\Delta\phi)^2$ definition by terms of order R^4

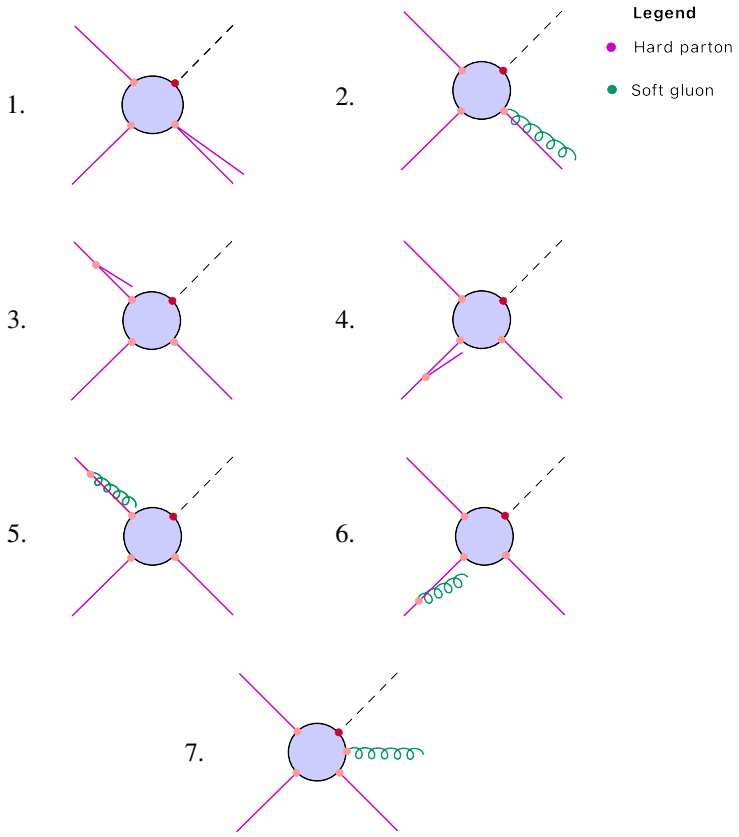

Figure 9: Soft/Collinear regions of the 3 - particle phase space

We refer to the contribution $\mathcal{J}$ as the jet function. Diagrams 3,4,5 and 6 represent the initial state radiation. This type of radiation is already present in the colour singlet production, we refer to it as σ_{ISR}. Finally, diagram 7 represents the soft radiation that is not clustered. This type of radiation enriches the singularity structure of the double real contribution and must therefore be included in the counterterm.

4.2 Counterterm

In the previous section, we briefly explained the relevant terms that enter into the calculation. In particular, we saw that the clustering procedure physically regulates configurations in which we have a final state collinear splitting. This means that we do not have to worry about these contributions when constructing the counterterm. The relevant types of singularities are then

- initial state radiation,
- soft radiation in the whole cut phase space (i.e. soft radiation that is not clustered).

We also subtract the soft limit of the collinear approximation to ensure we do not double count it.
As done in section (3) we can proceed by writing down the hadronic real emission cross section and then by approximating the real phase space and the matrix elements in the relevant IR singular regions. In full we would have

$$\begin{aligned}\sigma_{CT} = &\int_{\tau_{min}}^{1} d\tau \int_{\ln\sqrt{\tau}}^{-\ln\sqrt{\tau}} dy \lim_{q_T/Q\to 0} \int \frac{d\Phi_3^d}{2\hat{s}} \Theta(q_T - q_T^{\text{cut}}) \\ &\times \sum_{a,b} f_a(x_1) f_b(x_2) |\mathcal{M}^d_{ab\to cdH}|^2 \Theta(R_{3k} > R_0). \end{aligned} \tag{91}$$

Where c and d represent two generic final state partons.
The Θ-function in the second line of Eq. (91) ensures that we only consider unclustered configurations. This cut in the phase space introduces a new technical complication and, in particular, it will change the singularities due to soft radiation. However, hard initial state collinear radiation should not depend on the phase space cut. This is because by imposing a minimal transverse momentum $p_{3,T} > p_{3,T}^{cut}$ we are automatically separating the jet from the beam axis in p_T space.
The approximated real emission cross section for the process in equation (87) can be written as

$$\begin{aligned}\sigma_{CT} = &T_a^2(\sigma^{\text{out}}_{a,\text{coll}} - \sigma^{\text{out}}_{a,\text{coll}\to\text{soft}}) + T_b^2(\sigma^{\text{out}}_{b,\text{coll}} - \sigma^{\text{out}}_{b,\text{coll}\to\text{soft}}) \\ &+ T_a T_b \sigma^{\text{out}}_{\text{soft},ab} + T_a T_j \sigma^{\text{out}}_{\text{soft},aj} + T_b T_j \sigma^{\text{out}}_{\text{soft},bj} \,, \end{aligned} \tag{92}$$

where $T_{a(b)}$ and T_j represent the colour operators of the parton $a(b)$ and the jet respectively. The superscript "out" means that we are considering only radiation outside the jet cone (i.e. unclustered configurations). The above double real (or 2-jet) cross section is approximated in the sense that the matrix element square in equation (91) has

been replaced with the usual collinear/soft factorisation formula. In particular $\sigma^{\text{out}}_{a(b),\text{coll}}$ is obtained via the replacement

$$|\mathcal{M}^{d}_{ab\to cdH}|^2 \to |\mathcal{M}_{a(b),\text{coll}}|^2 = \frac{8\pi\alpha_s\mu^{2\epsilon}}{zp_{1(2)}\cdot k}\hat{P}(z,\epsilon)|\mathcal{M}_{\text{Born}}(zp_{1(2)},p_{2(1)},p_3,p_4))|^2\,, \tag{93}$$

where $\hat{P}(z,\epsilon)$ represents the adequate splitting function for the process under consideration. The terms $\sigma^{\text{out}}_{\text{soft},mn}$ are obtained via replacement of $|\mathcal{M}^{d}_{ab\to cdH}|^2$ with

$$|\mathcal{M}_{\text{soft},mn}|^2 = -8\pi\alpha_s\mu^{2\epsilon}\left(T_mT_n\frac{p_m\cdot p_n}{(p_m\cdot k)(p_n\cdot k)}\right)|\mathcal{M}_{\text{Born}}(p_1,p_2,p_3,p_4)|^2. \tag{94}$$

Finally $\sigma^{\text{out}}_{a(b),\text{coll}\to\text{soft}}$ is obtained from equation (93) by taking the $z\to 1$ limit. This matrix element can be written as

$$|\mathcal{M}_{a(b),\text{coll}\to\text{soft}}|^2 = 8\pi\alpha_s\mu^{2\epsilon}T^2_{1(2)}\frac{1}{p_{1(2)}\cdot k}\frac{p_1\cdot p_2}{(p_1+p_2)\cdot k}|\mathcal{M}_{\text{Born}}(p_1,p_2,p_3,p_4)|^2. \tag{95}$$

It is important to note that $\sigma^{\text{out}}_{a(b),\text{coll}} - \sigma^{\text{out}}_{a(b),\text{coll}\to\text{soft}}$ in equation (92) only contains hard collinear divergences. The singularity in this piece is thus independent on wheter the phase space is cut or not. This means that we can rewrite the approximated real emission cross section as

$$\begin{aligned}\sigma_{CT} = {} & T_a^2\sigma_{a,\text{coll}} + T_b^2\sigma_{b,\text{coll}} && (96)\\ & - T_a^2\sigma_{a,\text{coll}\to\text{soft}} - T_b^2\sigma_{b,\text{coll}\to\text{soft}} && (97)\\ & + T_aT_b\sigma^{\text{out}}_{\text{soft},ab} + T_aT_j\sigma^{\text{out}}_{\text{soft},aj} + T_bT_j\sigma^{\text{out}}_{\text{soft},bj} && (98)\end{aligned}$$

The terms in the line (96) represent the initial state radiation (ISR) and were already present in the colour singlet production discussed in the section (3.2). The terms in the lines (97)-(98) represent the conceptually new contributions to the counterterm due to the presence of a coloured parton in the final state.
In the following we will discuss these contributions and give the analytical formulae for them.

4.2.1 Initial state collinear counterterm

The derivation of the collinear counterterm

$$\sigma_{\text{ISR}} = T_a^2\sigma_{a,\text{coll}} + T_b^2\sigma_{b,\text{coll}} \tag{99}$$

can be done following the same reasoning as for the Higgs production case. In the appendix (A) we give the explicit formula for the d-dimensional 3-body phase space, necessary to derive the counterterm. To be definite, we present the explicit form of the initial state counterterms for the gluon-gluon channel only. This process receives contributions from two different subprocesses. The gluon-gluon splitting process

$$g(p_1) + g(p_2) \to H(p_3) + g(p_4) + g(p_5) \tag{100}$$

with

$$\sigma_{\mathrm{CT}}^{\mathrm{qg\text{-}split}} = \frac{\alpha_s}{\pi}\int_{\tau_{\min}}^{1} d\tau \int_{\log\sqrt{\tau}}^{-\log\sqrt{\tau}} dy f_g(x_2) \int \frac{d\Phi_B}{2\hat{s}} |\mathcal{M}_{gg\to Hg}|^2 \Bigg\{ \Bigg[\int_{x_1}^{1} \frac{dz}{z} P_{gg}(z) f_g\left(\frac{x_1}{z}\right) \tag{101}$$

$$- \frac{11C_A - 2n_f}{12} f_g(x_1) \Bigg] \tilde{L}_1(r_{\mathrm{cut}}) + \frac{C_A}{4} f_g(x_1) \tilde{L}_2(r_{\mathrm{cut}}) \Bigg\} + (x_1 \leftrightarrow x_2). \tag{102}$$

And the gluon to quark splitting

$$g(p_1) + g(p_2) \to H(p_3) + q(p_4) + \overline{q}(p_5) \tag{103}$$

with

$$\sigma_{\mathrm{CT}}^{\mathrm{qg\text{-}split}} = \frac{\alpha_s}{\pi}\int_{\tau_{\min}}^{1} d\tau \int_{\log\sqrt{\tau}}^{-\log\sqrt{\tau}} dy f_g(x_2) \int \frac{d\Phi_B}{2\hat{s}} |\mathcal{M}_{qg\to Hq}|^2 \tag{104}$$

$$\times \left\{ \int_{x_1}^{1} \frac{dz}{z} P_{qg}(z) f_g\left(\frac{x_1}{z}\right) \tilde{L}_1(r_{\mathrm{cut}}) \right\} 2n_f + (x_1 \leftrightarrow x_2). \tag{105}$$

4.2.2 Soft counterterm

For the explicit derivation of the soft counterterm we refer to Ref. [1].
It is possible to write the soft counterterm as the sum of three separate contributions:

$$\sigma_{CT}^{\mathrm{soft}} = \sigma_{\mathrm{BDC}}^{\mathrm{soft}} + \sigma_{\mathrm{mm}}^{\mathrm{soft}} + \sigma_{\mathrm{dec}}^{\mathrm{soft}}. \tag{106}$$

We call the first piece on the right hand side of equation (106) the "Born decoupling" since it contains the full dependence on the Born kinematics of $\sigma_{CT}^{\mathrm{soft}}$. The second term we call the "mismatch" since it appears only because we are insisting in writing the collinear radiation over the full phase space. The third term we call the "soft decoupled" piece. Next we will present the analytic formulas needed to compute this terms.

Born Decoupling

The Born decoupling contribution to the counterterm is given by

$$\sigma_{\mathrm{BDC}}^{\mathrm{soft}} = \frac{\alpha_s}{\pi}\sigma_{\mathrm{Born}} \frac{\tilde{L}_1(r_{\mathrm{cut}})}{2} (T_a^2 \log(\frac{t}{u}) + T_b^2 \log(\frac{u}{t})). \tag{107}$$

Note especially that this contribution vanishes if we are considering diagonal channels (like the gg- or $q\overline{q}$-channel) where $T_a^2 = T_b^2$.

Decoupled Mismatch

The mismatch piece is affected by the phase space cuts i.e. it has an explicit jet radius dependence. The full R dependent contribution can be written as

$$\sigma_{\mathrm{mm}}^{\mathrm{soft}} = \frac{\alpha_s}{\pi}\sigma_{\mathrm{Born}} \frac{\tilde{L}_1(r_{\mathrm{cut}})}{2} (-T_a^2 - T_b^2) I_{\mathrm{mm}}(R) \tag{108}$$

with

$$I_{\mathrm{mm}}(R) = \frac{2}{\pi}\int_{1-\frac{R^2}{2}}^{1} \frac{dx}{\sqrt{1-x^2}} \log(\xi(x)), \tag{109}$$

and

$$\xi(x) = 1 + \left(x - (1 - \frac{R^2}{2})\right) + \sqrt{\left(x - (1 - \frac{R^2}{2})\right)\left(x + (1 + \frac{R^2}{2})\right)}. \tag{110}$$

Notice in particular that the integral in equation (109) vanishes in the $R \to 0$ limit giving therefore a neglectable contribution for very small jet radii.

Decoupled Soft

The decoupled soft term contribution also explicitly depends on the jet radius and is given by

$$\sigma_{\text{dec}}^{\text{soft}} = \frac{\alpha_s}{\pi}\sigma_{\text{Born}}\frac{\tilde{L}_1(r_{\text{cut}})}{2}(-T_a T_j - T_b T_j) I_{\text{soft}}(R) \tag{111}$$

with

$$\begin{aligned} I_{\text{Soft}}(R) = &-\frac{2}{\pi}\log\left(R^2(1-\frac{R^2}{4})\right)\tan^{-1}\left(2\frac{\sqrt{1-\frac{R^2}{4}}}{R}\right) \\ &-\left[\frac{1}{\pi}\int_{1-\frac{R^2}{2}}^{1} dx \frac{\log(1-x^2)}{\sqrt{1-x^2}}\right] \\ &+\left[\frac{2}{\pi}\int_{1-\frac{R^2}{2}}^{1} 2dx \frac{x}{1-x^2}\tan^{-1}\left(\frac{\sqrt{1-x^2}}{\xi(x)-x}\right) - 2\log 2\right]. \end{aligned} \tag{112}$$

The leading R behaviour of the above integral can be found trough a Laurent expansion in R and is given by

$$I_{\text{soft}}(R) \approx \log(\frac{1}{R^2}) + \mathcal{O}(R). \tag{113}$$

Note in particular that the terms in the brackets in equation (112) only lead to power corrections in R.

4.2.3 Results

In this section we will present the results for the subtraction i.e.

$$\sigma_R^{H+1\text{-jet}}(R) - \sigma_{\text{CT,NLO}}^{H+1\text{-jet}}(R) \,. \tag{114}$$

As already discussed above, given a certain production channel, say the ab-channel, the full counterterm can be written as

$$\sigma_{\text{CT,NLO}}^{H+1\text{-jet}}(R) = \sigma_{\text{ISR},ab} + \sigma_{\text{BDC},ab}^{\text{soft}} + \sigma_{\text{mm},ab}^{\text{soft}}(R) + \sigma_{\text{dec},ab}^{\text{soft}}(R) \,, \tag{115}$$

with $\sigma_{\text{BDC},ab}^{\text{soft}}$ non-zero only for the non-diagonal channel qg.
In particular, as we will show explicitly, the counterterm involves full jet radius dependence. This means that the subtraction works for any jet radius used in experiments at the LHC.
All the plots shown in the following were generated via our own numerical program (`hjet_at_nlo`), which is publicly available at
`https://gitlab.com/mark.costantini/h_jet_nlo` .
In particular we use the `NNPDF31_nlo_as_0118` PDF set from [30]. The minimal transverse momentum of the jet is 30 GeV and the center of mass energy is 13 TeV.
In figure (10) we show the dependence of the full R subtracted piece on r_{cut} for the gg-channel and for different jet radii. By comparing these results with the ones obtained for Higgs production (see figure (7)) we see that the Higgs plus jet subtracted piece exhibits a much larger r_{cut} dependence. In particular, the power dependence at NLO is found to be linear as for the case of heavy quark pair production (see Refs. [13, 31, 32]). In general, the r_{cut} dependence is due to the power suppressed contributions that are left after the cancellation of the logarithmic singularity at small r_{cut} (a more detailed discussion can be found in Ref. [33] and references therein).
In figure (11) the performance of the leading R subtracted piece to converge to the full R extrapolated result is shown. In particular from the comparison of figures (10) and (11) it becomes clear that the leading R expansion of the counterterm only works for small jet radii like $R = 0.1$.
Finally in figure (12) we show the r_{cut} dependence of the subtracted piece for the qg- and qq'-channels.

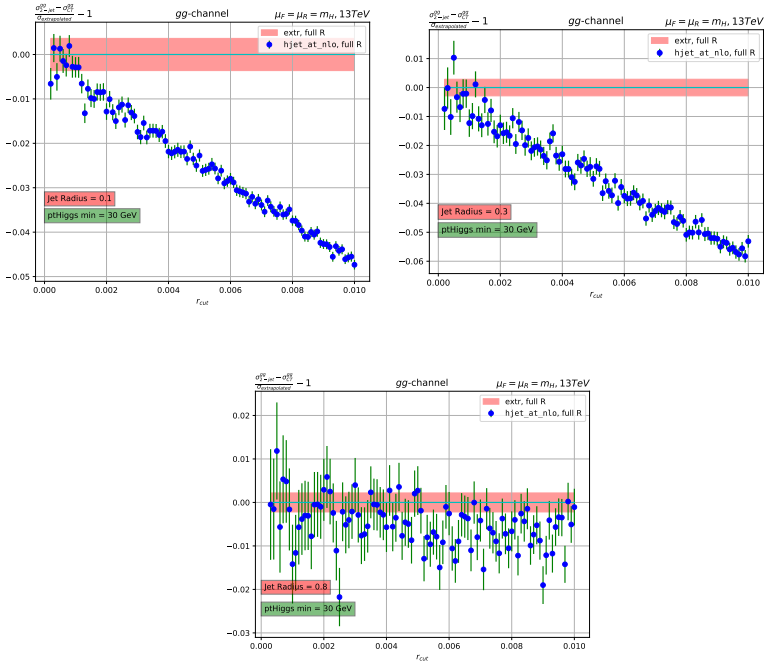

Figure 10: Dependence of the full R subtracted piece on r_{cut} for central scales and a $p_T^{\text{Higgs}} \geq 30$ GeV. The results for three different jet radii (0.1,0.3 and 0.8) are presented.

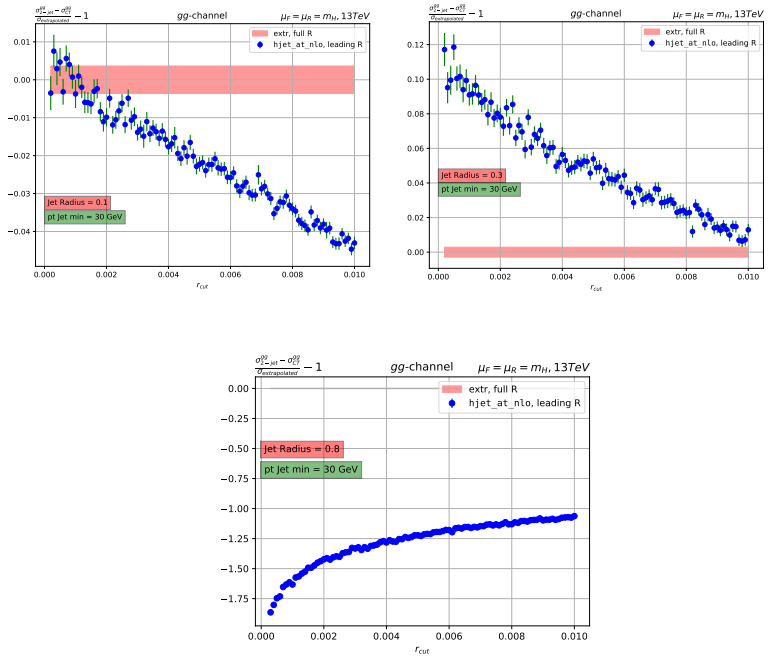

Figure 11: Dependence of the leading R subtracted piece (normalised w.r.t. the extrapolated full R result) on r_{cut} for central scales and a $p_T^{\text{Higgs}} \geq 30$ GeV. The results for three different jet radii (0.1,0.3 and 0.8) are presented.

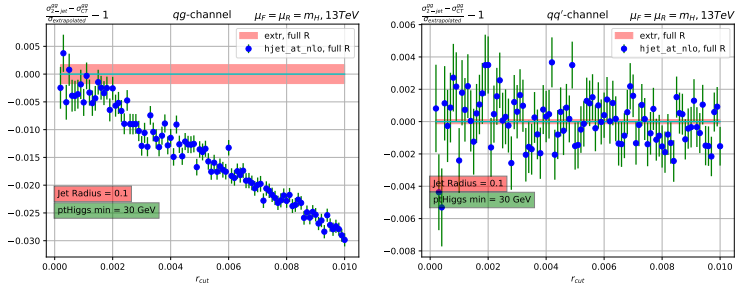

Figure 12: Dependence of the qg- and qq'-channels full R subtracted pieces (normalised w.r.t. the extrapolated full R result) on r_{cut} for central scales, $p_T^{\text{Higgs}} \geq 30$ GeV and $R = 0.1$.

4.3 $\mathcal{H}$-Function

To complete the NLO calculation we need to consider all the pieces that live at $q_T = 0$ i.e. all the pieces contributing to the 1-jet process. In the following we will present all these terms and give the explicit formulas for the gg-channel.

4.3.1 Born

The Born process clearly contributes to the $\mathcal{H}$-function since at this order the Higgs and the jet are exactly "back-to-back" thus giving $q_T = 0$. For the $gg \to Hg$ process, as for all other processes contributing to Higgs plus jet production at the same order in perturbation theory, the explicit formulas for the squared matrix elements can be found in Ref. [34].

4.3.2 Virtual, soft and jet-function contribution

In the section for the colour singlet production we have seen that the IR poles of the virtual correction exactly cancel with those of the subtraction operator in equation (78). For the case of Higgs plus jet production, the IR singular structure of the virtual contribution is known and can be found in equations (3.1)-(3.5) of Ref. [34]. However, the subtraction operator is no longer the same as for the colour singlet production. In particular, it receives contributions from the jet function and the soft counterterm.
The leading R behaviour of the jet function has been calculated in Ref. [35]. In particular, this calculation does not take into account the power corrections in R and is therefore only valid for small jet radii. Depending on whether we have a gluon or a quark as the leading jet with additional collinear radiation, we obtain a gluon- or quark-jet-function contribution, respectively. For the case of Higgs plus jet production in the gluon-gluon channel, we only have a gluon-jet-function contribution, written as:

$$\sigma_{\text{B}}^{gg} \otimes \mathcal{J}_g. \tag{116}$$

The gluon jet-function reads

$$\mathcal{J}_g = \frac{\alpha_s}{\pi}\left(\frac{Q^2}{\mu_R^2}\right)^{-\epsilon}\frac{1}{2}\Bigg\{\frac{C_A}{\epsilon^2} + \left(2C_A\frac{(11-\frac{2}{3}n_f)}{12} + C_A\log\left(\frac{1}{R^2}\right) + C_A\log\left(\frac{s^2}{tu}\right)\right)\frac{1}{\epsilon} + \mathcal{J}_1\Bigg\}\,, \tag{117}$$

where $\mathcal{J}_1$ is a finite contribution and is given by

$$\mathcal{J}_1 = \Bigg\{-\beta_0\log(R^2) + \frac{C_A}{4}\log^2(R^2) + \log\left(\frac{s^2}{tu}\right)\left(\beta_0 + \frac{C_A}{4}\log\left(\frac{s^2}{tu}\right) - \frac{C_A}{2}\log(R^2)\right) + C_A\left(\frac{67}{18} - \frac{23}{108}n_f - \frac{\pi^2}{3}\right)\Bigg\}, \tag{118}$$

with

$$\beta_0 = \frac{(11C_A - 2n_f)}{12}. \tag{119}$$

The contribution to the $\mathcal{H}$-function from the soft radiation has been computed in Ref. [1]. For this piece the full R dependence is known. However, since we are missing power corrections in the jet function anyway we only use the leading R terms. We thus add the following term to the $\mathcal{H}$-function

$$\sigma_B^{gg}\otimes(\Gamma_S + \Gamma_{\rm BDC})\,, \tag{120}$$

with

$$\begin{aligned}\Gamma_S &= \frac{\alpha_s}{\pi}\left(\frac{Q^2}{\mu_R^2}\right)^{-\epsilon}(T_aT_j + T_bT_j)\frac{1}{2\epsilon}\left(\log\left(\frac{1}{R^2}\right) + \frac{\epsilon}{2}\log^2(R^2)\right)\\ &\underbrace{=}_{gg-channel} \frac{\alpha_s}{\pi}\left(\frac{Q^2}{\mu_R^2}\right)^{-\epsilon}2C_A\frac{1}{2\epsilon}\left(\log\left(\frac{1}{R^2}\right) + \frac{\epsilon}{2}\log^2(R^2)\right)\,,\end{aligned} \tag{121}$$

and

$$\Gamma_{\rm BDC} = -\frac{\alpha_s}{\pi}\left(\frac{Q^2}{\mu_R^2}\right)^{-\epsilon}\frac{1}{2\epsilon}\left(T_a^2\log\left(\frac{t}{u}\right) + T_b^2\log\left(\frac{u}{t}\right)\right) \tag{122}$$

$$\underbrace{=}_{gg-channel} 0\,. \tag{123}$$

Taking into account the jet-function and the soft radiation contribution, we can write the subtraction operator for Higgs plus jet production in the gluon-gluon channel as

$$\tilde{I}_{gg}^{\rm Hjet,(1)} = -\frac{1}{4}\left(\frac{Q^2}{\mu_R^2}\right)^{-\epsilon}\Bigg\{\left(\frac{1}{\epsilon^2} + i\pi\frac{1}{\epsilon} - \frac{\pi^2}{12}\right)2C_A + \frac{2\beta_0}{\epsilon} \tag{124}$$

$$+ \frac{C_A}{\epsilon^2} + \left(2\beta_0 + C_A\log\left(\frac{1}{R^2}\right) + C_A\log\left(\frac{s^2}{tu}\right)\right)\frac{1}{\epsilon} \tag{125}$$

$$+ \frac{C_A}{\epsilon}\log\left(\frac{1}{R^2}\right)\Bigg\}\,. \tag{126}$$

The subtracted virtual is then defined as

$$\tilde{\mathcal{M}}_{gg}^{\text{Hjet},(1)} = [1 - \tilde{I}_{gg}^{\text{Hjet},(1)}]\mathcal{M}_{gg}^{\text{Hjet},(1)} \,. \tag{127}$$

Note in particular, that apart from the finite virtual contributions we also need to take into account the finite contributions coming from the jet-function and the integrated soft counterterm. For this purpose we define the hard factor

$$H_{gg}^{\text{Hjet},(1)} \equiv \frac{|\tilde{\mathcal{M}}_{gg}^{\text{Hjet},(1)}|^2}{|\tilde{\mathcal{M}}_{gg}^{\text{Hjet},(0)}|^2} + \mathcal{J}_1 + \frac{C_A}{2}\log^2(R^2) \,. \tag{128}$$

4.3.3 $\overline{MS}$ contribution

Conceptually, the $\overline{MS}$ contribution to the $q_T = 0$ cross section is equivalent to the colour singlet case discussed in equation (80). The only complication comes from the existence of more subprocesses. In particular for the gg-channel additional contributions need to be taken into account due to the gluon to quark splitting subprocesses. The full $\overline{MS}$ cross-section can then be written as

$$\overline{MS} = \left[\frac{\alpha_s}{\pi}\log\left(\frac{Q^2}{\mu_F^2}\right)(P_{gg}(z_1) + P_{gg}(z_2))\right) \tag{129}$$

$$+ \frac{\alpha_s}{\pi}\log\left(\frac{Q^2}{\mu_F^2}\right)2n_f(P_{qg}(z_1) + P_{qg}(z_2))\right) \tag{130}$$

$$+ \frac{\alpha_s}{\pi}2n_f(C_{qg}(z_1) + C_{qg}(z_2))\Big)\Big] \,, \tag{131}$$

where $C_{qg}(z) = \frac{1}{2}z(1-z)$ and can be found in [28].
We now have all the ingredients to compute the full $\mathcal{H}$-function:

$$\mathcal{H}_{gg}^{\text{Hjet},(1)} = \sigma_{gg}^{\text{Born}} \otimes \left(1 + \frac{\alpha_s}{\pi}H_{gg}^{\text{Hjet},(1)} - \frac{\alpha_s}{\pi}k\beta_0\log\left(\frac{Q^2}{\mu_R^2}\right) + \overline{MS}\right) \tag{132}$$

5 Results

Having discussed the content of equation (48) for the case of Higgs plus jet production, we will now present the complete NLO results. We use the `NNPDF31_nlo_as_0118` PDF set from [30]. The jet radius is fixed at $R = 0.1$, the minimal transverse momentum of the jet is 30 GeV and the center of mass energy is 13 TeV.
In figure (13) we show the r_{cut} dependence of the full NLO result (all the partonic channels contributing at this order combined) for different scales μ_R, μ_F.
As already stated in section (4.2.3) the r_{cut} dependence is linear as for the case of heavy quark pair production.
In the following table we compare the $r_{\text{cut}} = 0$ extrapolated result of q_T subtraction against the `MCFM` result for the 3 different scale variations

NLO [pb]	$\mu_F = \mu_R = m_H$	$\mu_F = \frac{m_H}{2}, \mu_R = 2m_H$	$\mu_F = 2m_H, \mu_R = \frac{m_H}{2}$
q_T subtraction	13.256 ± 0.034	11.162 ± 0.024	15.755 ± 0.05
`mcfm`	13.250 ± 0.007	11.140 ± 0.005	15.701 ± 0.01
LO [pb]	7.758 ± 0.007	5.900 ± 0.005	10.451 ± 0.01

The results are in agreement with the cross section computed with the Catani-Seymour subtraction formalism within a few sigmas thus providing a strong cross check on our result. Moreover, by comparing these results with the LO results we observe a K factor of approximately $K \approx 1.7$.

In figure (14)-(17) we compare the NLO differential distributions obtained with our own numerical program (in red) against those obtained with `MCFM` (in cyan). The q_T subtraction slicing parameter is $r_{\text{cut}} = 0.0003$ and the scales μ_F and μ_R are set to the central value $m_H \approx 125$ GeV.
In figure (14) we show the NLO differential distribution of the Higgs rapidity. From the graph it is clear that we find excellent agreement between our and the `MCFM` result for a rapidity range of $|y_H| \leq 1.5$ (i.e. where the bulk of the events are). The small discrepancy for larger values of the rapidity modulus is due to the lower statistics in these regions. A computationally more intensive simulation would therefore resolve the discrepancy. Furthermore, comparing the NLO distribution with the LO distribution (in orange) we still observe a K-factor of about 1.7.
In figure (15) and (16), where we plot the invariant mass of the Higgs plus jet pair and the transverse momentum of the Higgs respectively, it is interesting to note the change in the shape of the distribution for the kinematically allowed minimum values. In particular, for figure (16) we note that while at LO the Higgs was exactly back-to-back with the jet and thus had a sharp cut-off of the transverse momentum at 30 GeV, at NLO, due to the soft unclustered radiation, even smaller values of p_T are allowed.
Finally, in figure (17), we show the differential NLO distribution of the transverse momentum of the jet. Here again we find excellent agreement between our and the `MCFM` result. Furthermore, from the comparison of the NLO and the LO distributions we still observe a K-factor of approximately 1.7.

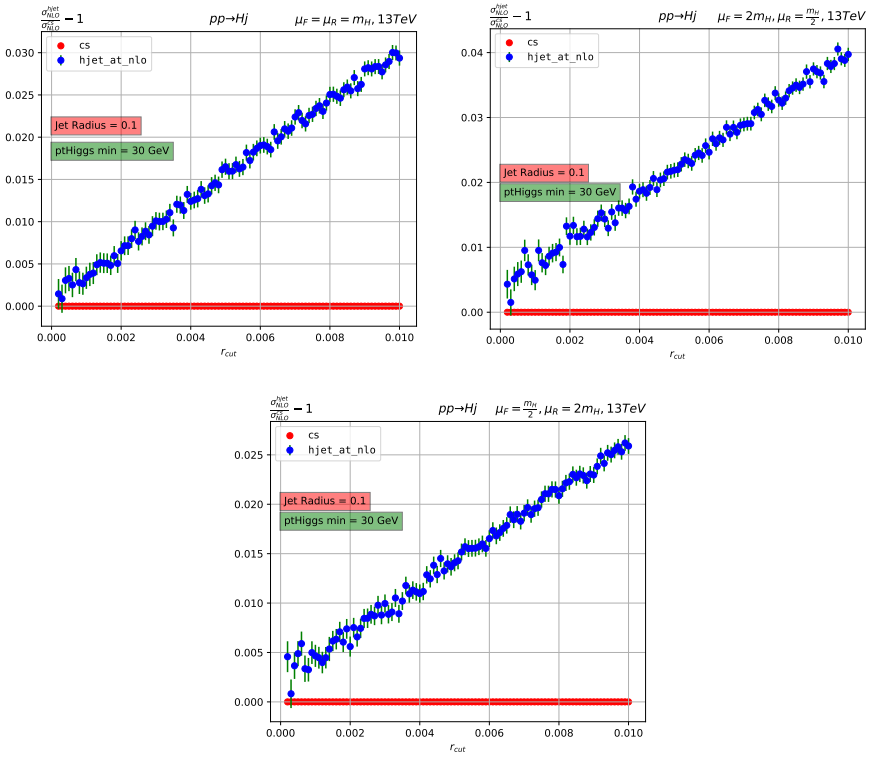

Figure 13: Dependence of the NLO $pp \to H + j + X$ cross section on $r_{cut} = q_T/Q$. The results are normalized to the r_{cut} - independent NLO cross section computed with Catani-Seymour subtraction

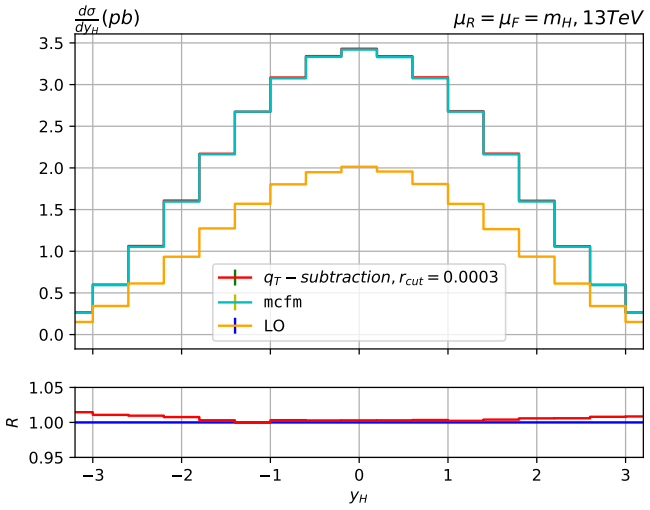

Figure 14: Rapidity distribution of the Higgs computed at NLO accuracy. Comparison of our result with the MCFM results.

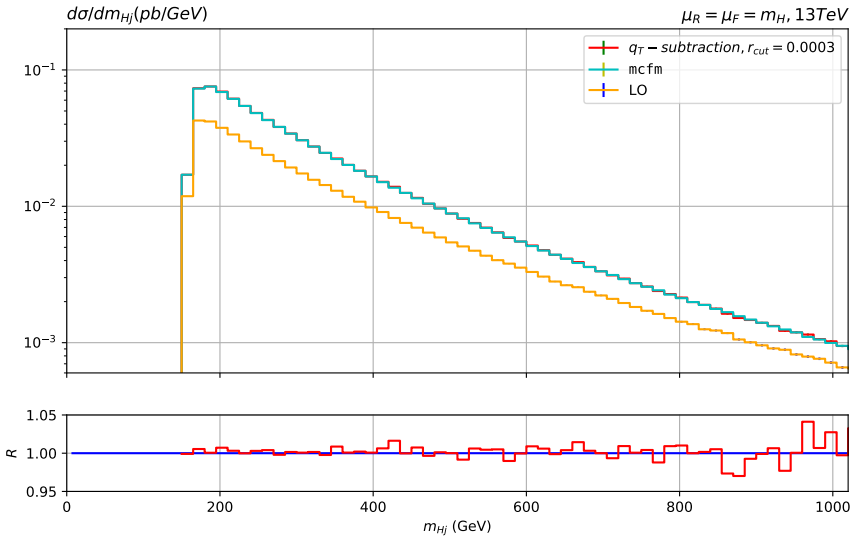

Figure 15: Invariant mass distribution of the Higgs + jet pair computed at NLO accuracy. Comparison of our result with the MCFM results.

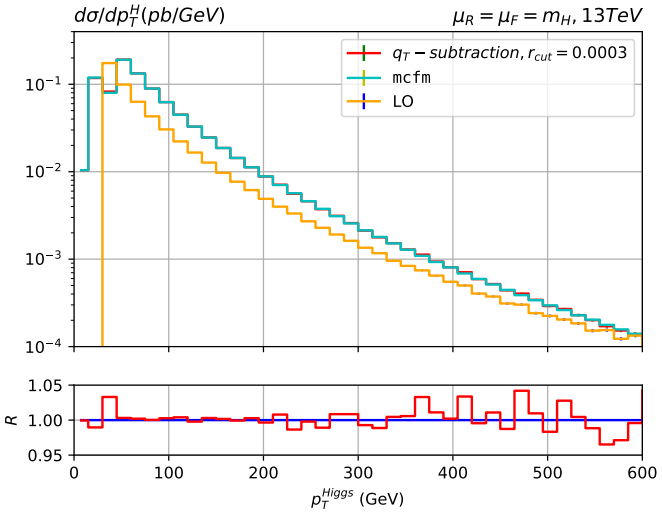

Figure 16: Transverse momentum distribution of the Higgs computed at NLO accuracy. Comparison of our result with the MCFM results.

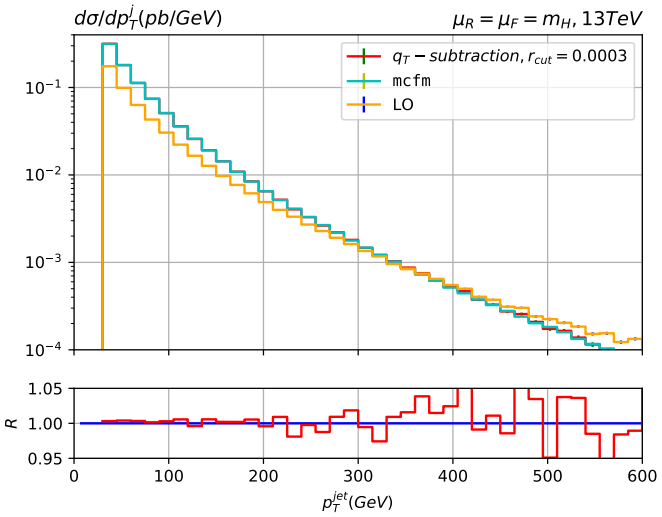

Figure 17: Transverse momentum distribution of the leading jet computed at NLO accuracy. Comparison of our result with the MCFM results.

6 Conclusions

Higgs plus jet production is a benchmark process at the LHC and represents an important observable for new physics searches. In this thesis we have computed the NLO corrections to this process within q_T subtraction. We now summarise our results.
In the chapter 2 we discussed the occurrence of IR divergences in perturbative QCD calculations and, in particular, introduced the factorisation properties of QCD matrix elements (at first order) in these singular limits. These properties are of fundamental importance in the computation of IR safe observables and are at the basis of most subtraction schemes. In chapter 3 we introduced the q_T subtraction scheme through the explicit example of Higgs production in gluon-gluon fusion at NLO. In particular, we discussed the correct identification of the q_T subtraction observable and presented all the analytical formulas needed for this NLO calculation.
Chapter 4 was devoted to the presentation of the extension of the q_T subtraction formalism for a process with a jet plus a massive colour singlet in the final state. We observed that a jet clustering algorithm is necessary for the q_T subtraction observable to regularise all IR singular regions. This, in particular, means that the subtraction explicitly depends on the jet radius. The calculation of the Higgs plus jet observable was divided into two parts: the counterterm and the $\mathcal{H}$-function. In particular, we saw that the counterterm involves the full dependence on R, while the contribution of the jet-function to the $\mathcal{H}$-function is only valid in the small R limit.
The full NLO cross section is therefore only valid in the small R limit. We explicitly verified this validity for jet radii $R \leq 0.1$. An important calculation, for the extension of the work done in this thesis, is therefore represented by the computation of the full R-dependent jet function.
Finally, in the chapter 5, we presented our results. The NLO cross section calculated with our numerical program agrees with the corresponding cross section obtained with `MCFM`. Moreover, we observe a linear dependence of the q_T subtraction NLO cross section on the slicing variable r_{cut} in contrast to the quadratic dependence of the colour singlet case. Finally, we compared our NLO results for various kinematical distributions with those obtained using the `MCFM` program, and found excellent agreement.

A 2 and 3 Particle Phase Space

In this appendix we show the explicit form of the two and three particle phase space employed to analytically integrate the collinear limit of the real emission cross section in section (3) and (4) respectively.
For the two particle case the kinematic is given by

$$p \to k + q \ , \ k^2 = 0 \ , \ q^2 = Q^2 \ , \ \hat{s} = p^2 \ , \ z = \frac{Q^2}{\hat{s}} \tag{133}$$

The two body phase space is defined as

$$\int d\Phi_2^d(k,q) = \int \frac{d^{d-1}\vec{k}}{(2\pi)^{d-1}2k^0} \frac{d^{d-1}\vec{q}}{(2\pi)^{d-1}2q^0} (2\pi)^d \delta^{(d)}(p-k-q). \tag{134}$$

Exploiting the c.o.m. frame semplifications this can be written as

$$\frac{1}{4(2\pi)^{d-2}} \int \frac{dk^0 (k^0)^{d-3} d\Omega_{d-1}}{\sqrt{(k^0)^2 + Q^2}} \delta(\sqrt{\hat{s}} - k^0 - \sqrt{(k^0)^2 + Q^2}) \tag{135}$$

$$= \frac{1}{4\sqrt{\hat{s}}(2\pi)^{d-2}} \left(\frac{\sqrt{\hat{s}}}{2}(1-z) \right)^{d-3} \int d\Omega_{d-2} \int_{-1}^{1} d\cos\theta (\sin\theta)^{d-4}, \tag{136}$$

where in the last step we solved the delta function and used:

$$d\Omega_{d-1} = d\Omega_{d-2} d\cos\theta (\sin\theta)^{d-4}.$$

Further, after a change of variables $\cos\theta \to x_T^2 = \frac{q_T^2}{Q^2}$

$$\cos\theta = \pm\sqrt{1 - \frac{4z x_T^2}{(1-z)^2}} \tag{137}$$

we get

$$\int d\Phi_2^d(k,q) = \frac{(\frac{4\pi^2}{Q^2})^\epsilon}{16\pi^2} \int d\Omega_{d-2} \int_0^{(x_T^{\max})^2} dx_T^2 (x_T^2)^{-\epsilon} \frac{z}{\sqrt{(1-z)^2 - 4z x_T^2}} \int_{-1}^{1} d\cos\theta (\delta^+ + \delta^-), \tag{138}$$

with $x_T^{\max} = \frac{1-z}{2\sqrt{z}}$. Note that the integral in $\cos\theta$ is necessary in order to separate the region in which $\cos\theta$ is negative from the positive one. In particular

$$\delta^+ \equiv \delta(\cos\theta - |\cos\theta(x_T)|), \tag{139}$$

$$\delta^- \equiv \delta(\cos\theta + |\cos\theta(x_T)|), \tag{140}$$

$$\text{with } \ |\cos\theta(x_T)| = \sqrt{1 - \frac{4z x_T^2}{(1-z)^2}} \ . \tag{141}$$

For the three body phase space we have the kinematics

$$p \to k + p_1 + p_2,\ \hat{s} = p^2,\ k^2 = 0,\ q_{12}^2 = (p_1 + p_2)^2 = Q^2. \tag{142}$$

Using the two body phase space decomposition (see for instance Hitoshi's notes on phase space) just once we get

$$\int d\Phi_3^d(k, p_1, p_2) = \int \frac{dQ^2}{2\pi} d\Phi_2^d(k, q_{12}) d\Phi_2^d(p_1, p_2). \tag{143}$$

where $d\Phi_2^d(k, q_{12})$ is the two particle phase space calculated above and $d\Phi_2^d(p_1, p_2)$ is the phase space for p_1 and p_2 in the frame where they are "back to back". We can therefore write

$$\int d\Phi_3^d(k, p_1, p_2) = \frac{\left(\frac{4\pi^2}{Q^2}\right)^\epsilon}{16\pi^2} \int_{Q^2_{\min}}^{Q^2_{\max}} \frac{dQ^2}{2\pi} \int d\Omega_{d-2} \int_0^{(x_T^{\max})^2} dx_T^2 (x_T^2)^{-\epsilon} \tag{144}$$

$$\times \frac{z}{\sqrt{(1-z)^2 - 4z x_T^2}} \int_{-1}^{1} d\cos\theta (\delta^+ + \delta^-) \int d\Phi_2^d(p_1, p_2)\ . \tag{145}$$

Acknowledgements

First and foremost I would like to warmly thank Prof. Massimiliano Grazzini for giving me the opportunity to work on my Master Thesis within his research group.
I particularly appreciate the way I was exposed to and involved in the stimulating and fascinating environment of the Department of Theoretical Particle Physics at the University of Zürich.
I would also like to express my profound gratitude to my two advisors Dr. Luca Buonocore and Dr. Luca Rottoli for their prompt and helpful answers to all my questions ranging from understanding QCD to more mathematical or programming problems. I really appreciated their "1 minute" of time because, even when they had a very busy schedule, they always found time to talk to me.
I am also very grateful to Jürg and Chiara for the useful discussions I had with them.
I want to thank my friends from Lettenstrasse 16 and 18 for all the time we spent together this year.
Last but not least, I want to thank my parents and sisters for the support and love I have always received.

References

[1] L. Buonocore, J. Haag, M. Grazzini, and L. Rottoli. In preparation. 2021.

[2] F. Englert and R. Brout. Broken Symmetry and the Mass of Gauge Vector Mesons. *Phys. Rev. Lett.*, 13:321–323, 1964.

[3] Peter W. Higgs. Broken Symmetries and the Masses of Gauge Bosons. *Phys. Rev. Lett.*, 13:508–509, 1964.

[4] Peter W. Higgs. Spontaneous Symmetry Breakdown without Massless Bosons. *Phys. Rev.*, 145:1156–1163, 1966.

[5] Yotam Soreq, Hua Xing Zhu, and Jure Zupan. Light quark Yukawa couplings from Higgs kinematics. *JHEP*, 12:045, 2016.

[6] Fady Bishara, Ulrich Haisch, Pier Francesco Monni, and Emanuele Re. Constraining Light-Quark Yukawa Couplings from Higgs Distributions. *Phys. Rev. Lett.*, 118(12):121801, 2017.

[7] Massimiliano Grazzini, Agnieszka Ilnicka, and Michael Spira. Higgs boson production at large transverse momentum within the SMEFT: analytical results. *Eur. Phys. J. C*, 78(10):808, 2018.

[8] Radja Boughezal, Christfried Focke, Walter Giele, Xiaohui Liu, and Frank Petriello. Higgs boson production in association with a jet at NNLO using jettiness subtraction. *Phys. Lett. B*, 748:5–8, 2015.

[9] Radja Boughezal, Fabrizio Caola, Kirill Melnikov, Frank Petriello, and Markus Schulze. Higgs boson production in association with a jet at next-to-next-to-leading order. *Phys. Rev. Lett.*, 115(8):082003, 2015.

[10] Xuan Chen, Thomas Gehrmann, Nigel Glover, and Alexander Huss. NNLO QCD Corrections for Higgs-plus-jet Production in the Four-lepton Decay Mode. *PoS*, RADCOR2019:003, 2019.

[11] Stefano Catani and Massimiliano Grazzini. An NNLO subtraction formalism in hadron collisions and its application to Higgs boson production at the LHC. *Phys. Rev. Lett.*, 98:222002, 2007.

[12] Massimiliano Grazzini, Stefan Kallweit, and Marius Wiesemann. Fully differential NNLO computations with MATRIX. *Eur. Phys. J. C*, 78(7):537, 2018.

[13] Stefano Catani, Simone Devoto, Massimiliano Grazzini, Stefan Kallweit, and Javier Mazzitelli. Top-quark pair production at the LHC: Fully differential QCD predictions at NNLO. *JHEP*, 07:100, 2019.

[14] Stefano Catani, Simone Devoto, Massimiliano Grazzini, Stefan Kallweit, and Javier Mazzitelli. Bottom-quark production at hadron colliders: fully differential predictions in NNLO QCD. *JHEP*, 03:029, 2021.

[15] Stefano Catani, Ignacio Fabre, Massimiliano Grazzini, and Stefan Kallweit. $t\bar{t}H$ production at NNLO: the flavour off-diagonal channels. *Eur. Phys. J. C*, 81(6):491, 2021.

[16] Luca Buonocore, Massimiliano Grazzini, Stefan Kallweit, Chiara Savoini, and Francesco Tramontano. Mixed QCD-EW corrections to $pp \to \ell\nu_\ell + X$ at the LHC. *Phys. Rev. D*, 103:114012, 2021.

[17] Roberto Bonciani, Luca Buonocore, Massimiliano Grazzini, Stefan Kallweit, Narayan Rana, Francesco Tramontano, and Alessandro Vicini. Mixed strong—electroweak corrections to the Drell—Yan process. 6 2021.

[18] T. Kinoshita. Mass singularities of Feynman amplitudes. *J. Math. Phys.*, 3:650–677, 1962.

[19] T. D. Lee and M. Nauenberg. Degenerate systems and mass singularities. *Phys. Rev.*, 133:B1549–B1562, Mar 1964.

[20] George Sterman and Steven Weinberg. Jets from quantum chromodynamics. *Phys. Rev. Lett.*, 39:1436–1439, Dec 1977.

[21] Gavin P. Salam. Towards Jetography. *Eur. Phys. J. C*, 67:637–686, 2010.

[22] Stefano Catani and Massimiliano Grazzini. Collinear factorization and splitting functions for next-to-next-to-leading order QCD calculations. *Phys. Lett. B*, 446:143–152, 1999.

[23] R. Keith Ellis, W. James Stirling, and B. R. Webber. *QCD and collider physics*, volume 8. Cambridge University Press, 2 2011.

[24] S. Catani and M. H. Seymour. The Dipole formalism for the calculation of QCD jet cross-sections at next-to-leading order. *Phys. Lett. B*, 378:287–301, 1996.

[25] Stefano Catani, Stefan Dittmaier, Michael H. Seymour, and Zoltan Trocsanyi. The Dipole formalism for next-to-leading order QCD calculations with massive partons. *Nucl. Phys. B*, 627:189–265, 2002.

[26] S. Frixione, Z. Kunszt, and A. Signer. Three jet cross-sections to next-to-leading order. *Nucl. Phys. B*, 467:399–442, 1996.

[27] Daniel de Florian and Massimiliano Grazzini. The Structure of large logarithmic corrections at small transverse momentum in hadronic collisions. *Nucl. Phys. B*, 616:247–285, 2001.

[28] Stefano Catani, Leandro Cieri, Daniel de Florian, Giancarlo Ferrera, and Massimiliano Grazzini. Universality of transverse-momentum resummation and hard factors at the NNLO. *Nucl. Phys. B*, 881:414–443, 2014.

[29] Massimiliano Grazzini, Stefan Kallweit, Stefano Pozzorini, Dirk Rathlev, and Marius Wiesemann. W^+W production at the LHC: fiducial cross sections and distributions in NNLO QCD. *JHEP*, 08:140, 2016.

[30] Richard D. Ball et al. Parton distributions from high-precision collider data. *Eur. Phys. J. C*, 77(10):663, 2017.

[31] Stefano Catani, Simone Devoto, Massimiliano Grazzini, Stefan Kallweit, Javier Mazzitelli, and Hayk Sargsyan. Top-quark pair hadroproduction at next-to-next-to-leading order in qcd. *Phys. Rev. D*, 99:051501, Mar 2019.

[32] Stefano Catani, Massimiliano Grazzini, and Hayk Sargsyan. Azimuthal asymmetries in QCD hard scattering: infrared safe but divergent. *JHEP*, 06:017, 2017.

[33] Luca Buonocore, Massimiliano Grazzini, and Francesco Tramontano. The q_T subtraction method: electroweak corrections and power suppressed contributions. *Eur. Phys. J. C*, 80(3):254, 2020.

[34] V. Ravindran, J. Smith, and W. L. Van Neerven. Next-to-leading order QCD corrections to differential distributions of Higgs boson production in hadron hadron collisions. *Nucl. Phys. B*, 634:247–290, 2002.

[35] Peng Sun, C. P. Yuan, and Feng Yuan. Transverse Momentum Resummation for Dijet Correlation in Hadronic Collisions. *Phys. Rev. D*, 92(9):094007, 2015.